Supersymmetric type-III seesaw mechanism: Lepton flavor violating decays and dark matter

J. N. Esteves[1,*] and J. C. Romao[1,†]

[1]*Departamento de Física and CFTP, Instituto Superior Técnico, Avenida Rovisco Pais 1, 1049-001 Lisboa, Portugal*

M. Hirsch[2,‡]

[2]*AHEP Group, Instituto de Física Corpuscular-C.S.I.C./Universitat de València,
Edificio de Institutos de Paterna, Apartado 22085, E-46071 València, Spain*

F. Staub[3,§] and W. Porod[3,‖]

[3]*Institut für Theoretische Physik und Astronomie, Universität Würzburg, Am Hubland, 97074 Wuerzburg*

We study a supersymmetric version of the seesaw mechanism type III. The model consists of the minimal supersymmetric extension of the standard model particle content plus three copies of **24** superfields. The fermionic part of the $SU(2)$ triplet contained in the **24** is responsible for the type-III seesaw, which is used to explain the observed neutrino masses and mixings. Complete copies of **24** are introduced to maintain gauge coupling unification. These additional states change the beta functions of the gauge couplings above the seesaw scale. Using minimal Supergravity boundary conditions, we calculate the resulting supersymmetric mass spectra at the electroweak scale using full 2-loop renormalization group equations. We show that the resulting spectrum can be quite different compared to the usual minimal Supergravity spectrum. We discuss how this might be used to obtain information on the seesaw scale from mass measurements. Constraints on the model space due to limits on lepton flavour violating decays are discussed. The main constraints come from the bounds on $\mu \to e\gamma$ but there are also regions where the decay $\tau \to \mu\gamma$ gives stronger constraints. We also calculate the regions allowed by the dark matter constraint. For the sake of completeness, we compare our results with those for the supersymmetric seesaw type II and, to some extent, with type I.

I. INTRODUCTION

Supersymmetry (SUSY) offers a number of advantages compared to the standard model (SM). To name just a few, SUSY has a dark matter candidate, it can alleviate the gauge hierarchy problem, and the minimal supersymmetric extension of the standard model (MSSM) leads to gauge coupling unification, if SUSY particles exist with masses of the order of the electroweak scale. However, in the MSSM neutrino masses are zero, just as in the SM. Neutrino oscillation experiments [1–4], on the other hand, have shown that neutrinos have tiny, but nonzero, masses and that mixing in the leptonic sector is large [5].

From a theoretical point of view, if neutrinos are Majorana particles, *all* models of neutrino mass at low energies reduce to the unique dimension-5 operator [6]

$$(m^\nu)_{\alpha\beta} = \frac{f_{\alpha\beta}}{\Lambda}(HL)(HL). \tag{1}$$

Neutrino experiments determine only $f_{\alpha\beta}/\Lambda$ but contain no information about the origin of this operator nor about

the absolute size of Λ. If f is a coefficient $\mathcal{O}(1)$, current neutrino data indicates $\Lambda \lesssim \mathcal{O}(10^{15})$ GeV. This is the essence of the "seesaw" mechanism.

One can show that there are exactly three different tree-level realizations of the seesaw mechanism [7]. Type-I is the well-known case of the exchange of a heavy fermionic singlet [8–10]. Type-II corresponds to the exchange of a scalar $SU(2)$ triplet [11,12]. In seesaw type-III one adds (at least two) fermionic $SU(2)$ triplets to the field content of the SM [13]. If in case of type-II and type-III models one would extend the usual MSSM by just the superfields responsible for neutrino masses and mixings, one would destroy the nice feature of gauge coupling unification as they belong to incomplete $SU(5)$ representations. This problem is easily cured by embedding the new states in complete $SU(5)$ representations, e.g. in case of type-II in **15** plets [14] and in case of type-III in **24** plets [15]. Note, that the **24** plet contains beside the $SU(2)$ triplet also a singlet state, which also contributes to neutrino physics, and, thus, one has in this case actually a mixture between type-I and type-III.

Understanding the nature of supersymmetry breaking by measuring the soft parameters will be one of the central tasks if signals of SUSY are found at the LHC. All the more so, since one can possibly gain some insight into the high energy scale physics from such measurements. Two kinds

---
*joaomest@cftp.ist.utl.pt
† jorge.romao@ist.utl.pt
‡ mahirsch@ific.uv.es
§ florian.staub@physik.uni-wuerzburg.de
‖ porod@physik.uni-wuerzburg.de

of measurements containing indirect information about the seesaw scale in SUSY models exist in principle: lepton flavour violating (LFV) observables and sparticle masses. In case of seesaw type-I, low-energy LFV decays such as $l_i \rightarrow l_j + \gamma$ and $l_i \rightarrow 3l_j$ have been calculated in [16–25]; $\mu - e$ conversion in nuclei has been studied in [26,27]. The type-II model has received less attention, although it has actually fewer free parameters than type-I implying that ratios of LFV decays of leptons can actually be predicted as a function of neutrino angles in mSUGRA, as has been shown in [14,28]. A first study has been done in [29]. We stress that such a setup can not explain neutrino data unless nonrenormalizable operators are added, as indeed is done in [29]. This is due to the need of generating a sufficiently large splitting between the Yukawa couplings of the singlet and the triplets, which can not be obtained from Renormalization Group Equation (RGE) running only. Moreover, in the above publications for the type-II and type-III models only 1-loop RGEs have been used. However, we will show that using 2-loop RGEs is important for the calculation of the spectrum as this leads to a shift of the Grand Unified Theory (GUT) scale.

Measurements at colliders, once SUSY is discovered, can provide additional information. LFV decays of left sleptons within mSUGRA have been studied for type-I in [30,31] and for type-II in [28,31]. Precise mass measurements, in particular, of the sleptons and sneutrinos, might also show indirect effects of the seesaw [32–34]. As mentioned above, the additional heavy states of type-II and type-III lead to changes in the running of the beta functions and also of the mass parameters above the seesaw scale leading to changes of the spectrum at the electroweak scale compared to the usual mSUGRA expectations. From different combinations of masses one can form "invariants", i.e. numbers which to leading order depend only on the seesaw scale [15], although there are important corrections at 2 loop for the type-II [28] and, as we will show in this paper, also for type-III. It is also interesting to note that the additional Yukawa couplings at the high scale can lead to a mass splitting between smuons and selectrons, which in principle can be measured at the LHC; it has been shown in Ref. [35] that such a splitting may be constrained down to $\mathcal{O}(10^{-4})$ for 30 fb^{-1} of integrated luminosity. In mSUGRA, one expects this splitting to be tiny, whereas in mSUGRA plus seesaw significantly different masses are generated, as has been shown for type-I in Ref. [36].

The modified spectrum also affects the calculation of the relic density. Assuming the standard thermal history of the early universe only four very specific regions in parameter space of mSUGRA can correctly explain the most recent WMAP data [37]. These are (i) the bulk region; (ii) the coannihilation line; (iii) the "focus point" line and (iv) the "Higgs funnel" region. In the bulk, where the SUSY particles are relatively light, no specific relations among the sparticle masses exist. In the coannihilation line the

lightest scalar tau is nearly degenerate with the lightest neutralino, thus reducing the neutralino relic density with respect to naive expectations [38,39]. In the focus point line [39,40], $\Omega_{\tilde{\chi}_1^0} h^2$ is small enough to explain $\Omega_{\mathrm{DM}} h^2$ due to a rather small value of μ leading to an enhanced Higgsino component in the lightest neutralino and thus an enhanced coupling to the Z boson. Lastly, at large $\tan\beta$ an s channel resonance pair annihilation of neutralinos through the CP-odd Higgs boson can become important. This is called the "Higgs funnel" region [41]. Also in the seesaw models of type-II and III these regions exist but the regions get shifted. Moreover, if the seesaw scale is sufficiently low the coannihilation region disappears in type-II models [42]. We will show that the same happens in case of the type-III model, and we will contrast the results of this model with type-I and type-II models.

The rest of this paper is organized as follows. In the next section, we first define the model. For completeness, and since we will compare the results for the different variants, we give the definitions for minimal type-I and type-II seesaws as well. We have used SARAH [43–45] to calculate the full 2-loop RGEs, based on the general expressions given in [46]. We have, where possible, compared our results to previously available work and generally found agreement. However, [47] has calculated 1-loop RGEs for all parameters and found some differences in case of the seesaw type-II to the RGEs published in [14]. Our calculation agrees with [47]. We then turn to the discussion of the resulting SUSY spectrum. The large changes in the spectrum affect the predictions for the rates of rare lepton decays, such as $\mu \rightarrow e\gamma$, and the relic density as discussed in Sec. III. We present in Sec. IV our conclusions. In the appendix, we first summarize the procedure on how to obtain the RGEs for the soft SUSY-breaking parameters from the beta functions and anomalous dimensions. We then give the formulas at the 1-loop and 2-loop level for these quantities for the seesaw models of type-II and type-III for an arbitrary number of new seesaw particles, which are decomposed according to their SM gauge quantum numbers.

II. MODELS AND SPECTRA

In this section, we briefly recall the main features of the three seesaw models. In models of type-II and III, one adds particles charged under the SM gauge group. As they correspond to incomplete $SU(5)$ representations, they would destroy the nice feature of gauge coupling unification. For this reason we add at the seesaw scale(s) additional particles to obtain complete $SU(5)$ representations, which we briefly review below. A more detailed discussion including the embedding in $SU(5)$ models can be found in [47].

In the subsequent sections, we present the various superpotentials. In addition, there will also be the corresponding soft SUSY terms which, however, reduce at the electroweak scale to the MSSM one and, thus, are not discussed

further. The additional terms of the soft SUSY-breaking potential, due to the heavy particles, do not effect the discussion presented later on, as their effect is at most of the order $M_{\mathrm{EWSB}}/M_{\mathrm{seesaw}}$ and, thus, can be safely neglected. In this paper, we will assume common soft SUSY breaking at the GUT scale M_{GUT} to specify the spectrum at the electroweak scale: a common gaugino mass $M_{1/2}$, a common scalar mass m_0, and the trilinear coupling A_0, which gets multiplied by the corresponding Yukawa couplings to obtain the trilinear couplings in the soft SUSY-breaking Lagrangian. In addition, the sign of the μ parameter is fixed, as is $\tan\beta = v_u/v_d$ at the electroweak scale, where v_d and v_u are the vacuum expectation values (vevs) of the neutral component of H_d and H_u, respectively. The models discussed below also contain new bilinear parameters in the superpotential leading to additional bilinear terms in the soft SUSY-breaking potential, which are proportional to B_0 of the MSSM Higgs sector. The corresponding RGEs decouple, and their only effect is a small mass splitting between the new heavy scalar particles from the new heavy fermionic states of the order B_0/M_{seesaw}. This leads to a tiny effect in the calculation of the thresholds at the seesaw scale(s) [48], which, however, we can safely neglect.

A. Supersymmetric seesaw type-I

In the case of seesaw type-I, one postulates very heavy right-handed neutrinos yielding the following superpotential below M_{GUT}:

$$W_I = W_{\mathrm{MSSM}} + W_\nu, \tag{2}$$

$$W_{\mathrm{MSSM}} = \hat{U}^c Y_u \hat{Q} \cdot \hat{H}_u - \hat{D}^c Y_d \hat{Q} \cdot \hat{H}_d - \hat{E}^c Y_e \hat{L} \cdot \hat{H}_d + \mu \hat{H}_u \cdot \hat{H}_d, \tag{3}$$

$$W_\nu = \hat{N}^c Y_\nu \hat{L} \cdot \hat{H}_u + \frac{1}{2} \hat{N}^c M_R \hat{N}^c, \tag{4}$$

where $A \cdot B = A_1 B_2 - A_2 B_1$ denotes the $SU(2)$ invariant product of two $SU(2)$ doublets. This model can be embedded in an $SU(5)$ using the following $SU(5)$ matter representations: $1 = N^c$, $\bar{5}_M = \{D^c, L\}$, and $10_M = \{Q, U^c, E^c\}$. For the neutrino mass matrix one obtains the well-known formula

$$m_\nu = -\frac{v_u^2}{2} Y_\nu^T M_R^{-1} Y_\nu. \tag{5}$$

Being complex symmetric, the light Majorana neutrino mass matrix in Eq. (5), is diagonalized by a unitary 3×3 matrix U [11]

$$\hat{m}_\nu = U^T \cdot m_\nu \cdot U. \tag{6}$$

Inverting the seesaw equation, Eq. (5), allows to express Y_ν as [49]

$$Y_\nu = \sqrt{2}\frac{i}{v_u}\sqrt{\hat{M}_R} \cdot R \cdot \sqrt{\hat{m}_\nu} \cdot U^\dagger, \tag{7}$$

where the $\hat{m}_\nu$ and $\hat{M}_R$ are diagonal matrices containing the corresponding eigenvalues. R is in general a complex orthogonal matrix. Note that, in the special case $R = \mathbf{1}$, Y_ν contains only "diagonal" products $\sqrt{M_i m_i}$. For U we will use the standard form

$$U = \begin{pmatrix} c_{12}c_{13} & s_{12}c_{13} & s_{13}e^{-i\delta} \\ -s_{12}c_{23} - c_{12}s_{23}s_{13}e^{i\delta} & c_{12}c_{23} - s_{12}s_{23}s_{13}e^{i\delta} & s_{23}c_{13} \\ s_{12}s_{23} - c_{12}c_{23}s_{13}e^{i\delta} & -c_{12}s_{23} - s_{12}c_{23}s_{13}e^{i\delta} & c_{23}c_{13} \end{pmatrix} \times \begin{pmatrix} e^{i\alpha_1/2} & 0 & 0 \\ 0 & e^{i\alpha_2/2} & 0 \\ 0 & 0 & 1 \end{pmatrix} \tag{8}$$

with $c_{ij} = \cos\theta_{ij}$ and $s_{ij} = \sin\theta_{ij}$. The angles θ_{12}, θ_{13}, and θ_{23} are the solar neutrino angle, the reactor (or CHOOZ) angle, and the atmospheric neutrino mixing angle, respectively. δ is the Dirac phase and α_i are Majorana phases. In the following, we will set the latter to 0 and consider in case of δ only the cases 0 and π.

B. Supersymmetric seesaw type-II

In seesaw models of type-II, one adds a scalar $SU(2)$ triplet T to generate neutrino masses. As this triplet carries also hypercharge one has to embed it in a 15 plet of $SU(5)$ which has under $SU(3) \times SU(2) \times U(1)$ the following decomposition [14]

$$\mathbf{15} = S + T + Z,$$

$$S \sim \left(6, 1, -\frac{2}{3}\right), \quad T \sim (1, 3, 1), \quad Z \sim \left(3, 2, \frac{1}{6}\right). \tag{9}$$

One has to add two **15** plets 15 and $\overline{15}$ to avoid a chiral anomaly below the GUT-scale. The $SU(5)$ invariant superpotential reads as

$$W = \frac{1}{\sqrt{2}}\mathbf{Y}_{15}\bar{5} \cdot 15 \cdot \bar{5} + \frac{1}{\sqrt{2}}\lambda_1 \bar{5}_H \cdot 15 \cdot \bar{5}_H$$

$$+ \frac{1}{\sqrt{2}}\lambda_2 5_H \cdot \overline{15} \cdot 5_H + \mathbf{Y}_5 10 \cdot \bar{5} \cdot \bar{5}_H$$

$$+ \mathbf{Y}_{10}10 \cdot 10 \cdot 5_H + M_{15}15 \cdot \overline{15} + M_5 \bar{5}_H \cdot 5_H \tag{10}$$

with $5_H = (H^c, H_u)$ and $\bar{5}_H = (\bar{H}^c, H_d)$. We do not show the part responsible for the $SU(5)$ breaking as we take the $SU(5)$ only as a guideline to fix some of the boundary conditions at M_{GUT}. Below M_{GUT} in the $SU(5)$-broken phase the superpotential reads

$$W_{II} = W_{MSSM} + \frac{1}{\sqrt{2}}(Y_T \hat{L} \hat{T}_1 \hat{L} + Y_S \hat{D}^c \hat{S}_1 \hat{D}^c) + Y_Z \hat{D}^c \hat{Z}_1 \hat{L}$$

$$+ \frac{1}{\sqrt{2}}(\lambda_1 \hat{H}_d \hat{T}_1 \hat{H}_d + \lambda_2 \hat{H}_u \hat{T}_2 \hat{H}_u) + M_T \hat{T}_1 \hat{T}_2$$

$$+ M_Z \hat{Z}_1 \hat{Z}_2 + M_S \hat{S}_1 \hat{S}_2, \qquad (11)$$

where fields with index 1 (2) originate from the 15 plet ($\overline{15}$ plet). The second term in Eq. (11) is responsible for the generation of the neutrino masses yielding

$$m_\nu = \frac{v_u^2}{2} \frac{\lambda_2}{M_T} Y_T. \qquad (12)$$

Note that

$$\hat{Y}_T = U^T \cdot Y_T \cdot U, \qquad (13)$$

i.e. Y_T is diagonalized by the same matrix as m_ν. If all neutrino eigenvalues, angles, and phases were known, Y_T would be fixed up to an overall constant which can be easily estimated to be

$$\frac{M_T}{\lambda_2} \simeq 10^{15} \text{ GeV}\left(\frac{0.05 \text{ eV}}{m_\nu}\right). \qquad (14)$$

In addition, there are the couplings Y_S and Y_Z, which, in principle, are not determined by any low-energy data. In the calculation of LFV observables in supersymmetry, both matrices, Y_T and Y_Z, contribute. Having a GUT model in mind, we require for the numerical discussion later the $SU(5)$ boundary conditions, apart from threshold corrections, $Y_T = Y_S = Y_Z$ at M_{GUT}.

As long as $M_Z \sim M_S \sim M_T \sim M_{15}$ gauge coupling unification will be maintained. The equality need not be exact for successful unification. In our numerical studies, we have taken into account the different running of these mass parameters, but we decouple them all at the scale $M_T(M_T)$ because the differences are small.

C. Supersymmetric seesaw type-III

In the case of a seesaw model type-III, one needs new fermions Σ at the high scale belonging to the adjoint representation of $SU(2)$. This has to be embedded in a **24** plet to obtain a complete $SU(5)$ representation. The superpotential of the unbroken $SU(5)$ relevant for our discussion is

$$W = \sqrt{2}\bar{5}_M Y^5 10_M \bar{5}_H - \frac{1}{4} 10_M Y^{10} 10_M 5_H + 5_H 24_M Y_N^{III} \bar{5}_M$$

$$+ \frac{1}{2} 24_M M_{24} 24_M. \qquad (15)$$

As above, we have not specified the Higgs sector responsible for the $SU(5)$ breaking. The new parts, which will give the seesaw mechanism, comes from the 24_M. It decomposes under $SU(3) \times SU(2) \times U(1)$ as

$$24_M = (1, 1, 0) + (8, 1, 0) + (1, 3, 0) + (3, 2, -5/6)$$

$$+ (3^*, 2, 5/6), = \hat{B}_M + \hat{G}_M + \hat{W}_M + \hat{X}_M + \hat{\bar{X}}_M. \qquad (16)$$

The fermionic components of (1,1,0) and (1,3,0) have exactly the same quantum numbers as $\hat{N}^c$ and Σ. Thus, the 24_M always produces a combination of the type-I and type-III seesaw.

In the $SU(5)$ broken phase the superpotential becomes

$$W_{III} = W_{MSSM} + \hat{H}_u\left(\hat{W}_M Y_W - \sqrt{\frac{3}{10}}\hat{B}_M Y_B\right)\hat{L}$$

$$+ \hat{H}_u \hat{\bar{X}}_M Y_X \hat{D}^c + \frac{1}{2}\hat{B}_M M_B \hat{B}_M + \frac{1}{2}\hat{G}_M M_G \hat{G}_M$$

$$+ \frac{1}{2}\hat{W}_M M_W \hat{W}_M + \hat{X}_M M_X \hat{\bar{X}}_M \qquad (17)$$

As before we use at the GUT scale the boundary condition $Y_W = Y_B = Y_X$ and $M_B = M_G = M_W = M_X$. Integrating out the heavy fields yields the following formula for the neutrino masses at the low scale:

$$m_\nu = -\frac{v_u^2}{2}\left(\frac{3}{10}Y_B^T M_B^{-1} Y_B + \frac{1}{2}Y_W^T M_W^{-1} Y_W\right). \qquad (18)$$

As mentioned above, there are two contributions stemming from the gauge singlet as well as from the $SU(2)$ triplet. In this case, the calculation of the Yukawa couplings in terms of a given high scale spectrum is more complicated than in the other two types of seesaw models. However, as we start from universal couplings and masses at M_{GUT}, we find that at the seesaw scale one still has $M_B \simeq M_W$ and $Y_B \simeq Y_W$ so that one can write in a good approximation

$$m_\nu = -v_u^2 \frac{4}{10} Y_W^T M_W^{-1} Y_W, \qquad (19)$$

and one can use the corresponding decomposition for Y_W as discussed in Sec. II A up to the overall factor 4/5.

D. Effects of the heavy particles on the MSSM spectrum

The appearance of charged particles at scales between the electroweak scale and the GUT scale leads to changes in the beta functions of the gauge couplings [14,15]. In the MSSM, the corresponding values at 1-loop level are $(b_1, b_2, b_3) = (33/5, 1, -3)$. In case of one **15** plet the additional contribution is $\Delta b_i = 7/2$, whereas in case of **24** plet it is $\Delta b_i = 5$. This results in case of type-II in a total shift of $\Delta b_i = 7$ for the minimal model and in case of type-III in $\Delta b_i = 15$ assuming 3 generations of **24** plets. This does not only change the evolution of the gauge couplings but also the evolution of the gaugino and scalar mass parameters with profound implications on the spectrum [15,28]. Additional effects on the spectrum of the scalars can be present if some of the Yukawa couplings get large [28,29,50], which can also happen in type-I models

[51]. In Fig. 1, we exemplify this by showing the values of selected mass parameters at $Q = 1$ TeV versus the seesaw scale for fixed high scale parameters $m_0 = M_{1/2} = 1$ TeV, and we have set the additional Yukawa couplings to zero. As expected, the effects in case of models of type-II and III are larger the smaller the corresponding seesaw-scale is. The scalar mass parameters shown are of the first generation, and, thus, the results are nearly independent of $\tan\beta$ and A_0. For illustration, we show in Fig. 2 the corresponding spectrum, where we have fixed $\tan\beta = 10$ and $A_0 = 0$.

We note that in all three model types the ratio of the gaugino mass parameters is nearly the same as in the usual mSUGRA scenarios but the ratios of the sfermion mass parameters change [15,28]. One can form four invariants for which at least at the 1-loop level the dependence on $M_{1/2}$ and m_0 is rather weak, e.g. $(m_L^2 - m_E^2)/M_1^2$, $(m_Q^2 - m_E^2)/M_1^2$, $(m_D^2 - m_L^2)/M_1^2$, and $(m_Q^2 - m_U^2)/M_1^2$. Here one could replace M_1 by any of the other two gaugino masses, which simply would amount in an overall rescaling. In Fig. 3, we show these invariants in the leading-log approximation at 1-loop order to demonstrate the principal behavior for seesaw type-II with a pair of **15** plets and seesaw type-III with three **24** plets. From this one concludes that in principle one has a handle to obtain information on the seesaw scale for given assumptions on the underlying neutrino mass model, if universal boundary conditions are assumed. For the type-I, i.e. singlets only, of course $\Delta b_i = 0$ and no change with respect to mSUGRA are expected. If, for example, the seesaw III model would be realized in nature with three **24** plets having similar masses around 10^{13} GeV, one could e.g. show that the corresponding ratios cannot be obtained with one pair of **15** plets in the seesaw II model, thus excluding this possibility. However, taking the seesaw II with two pairs of **15** plets,

one would obtain similar ratios as in this case the corresponding additional beta functions at 1-loop would be $\Delta b_i = 14$, e.g. nearly equal to our seesaw III model.

The leading-log approximation gives only the general trend, but there is an important dependence on the SUSY point chosen. In Fig. 4, we show as illustration $(m_L^2 - m_E^2)/M_1^2$ and $(m_Q^2 - m_E^2)/M_1^2$ for different mSUGRA points and at different loop orders: the dashed lines are at 1-loop level, whereas the solid ones are at 2-loop level. The points considered are Snowmass Point and Slopes3 (SPS3) [52] with $m_0 = 90$ GeV, $M_{1/2} = 400$ GeV, $A_0 = 0$, $\tan\beta = 10$, $\mu > 0$ and for the same values of A_0 and $\tan\beta$ two points with $M_{1/2} = 1$ TeV: $m_0 = 500$ GeV and $m_0 = 1$ TeV. The black line shows for comparison the leading-log approximation. We observe that usually the approximation gets worse for lower values of M_{24}, and this is even stronger at the 2-loop level, which is a consequence of the large coefficient in the beta functions at the 2-loop level, see e.g. Appendix A 4. Nevertheless, one sees that in general it gives the correct trend, but it might even fail completely, e.g. in the case of $M_{1/2} = m_0 = 1$ TeV. The reason for the drop around $M_{24} \simeq 3.5 \times 10^{13}$ is that the difference between the parameters goes to zero as can also be seen from the right of Fig. 1, see also discussion below.

Last, but not least, we note that the use of the 2-loop RGEs leads to a shift of $M_{\rm GUT}$ from about 2×10^{16} GeV for **24**-plet mass of 10^{16} GeV to about 4×10^{16} GeV for **24**-plet mass of 10^{13} GeV, which is part of the differences between the 1-loop and 2-loop results in Fig. 4. Here, $M_{\rm GUT}$ is defined as the scale where the electroweak couplings meet, e.g. $g_{U(1)} = g_{SU(2)}$. This implies also that there is some difference for the strong coupling, which is, however, in the order of 5–10%, which can easily be accounted for by threshold effects of the new GUT particles, e.g. the
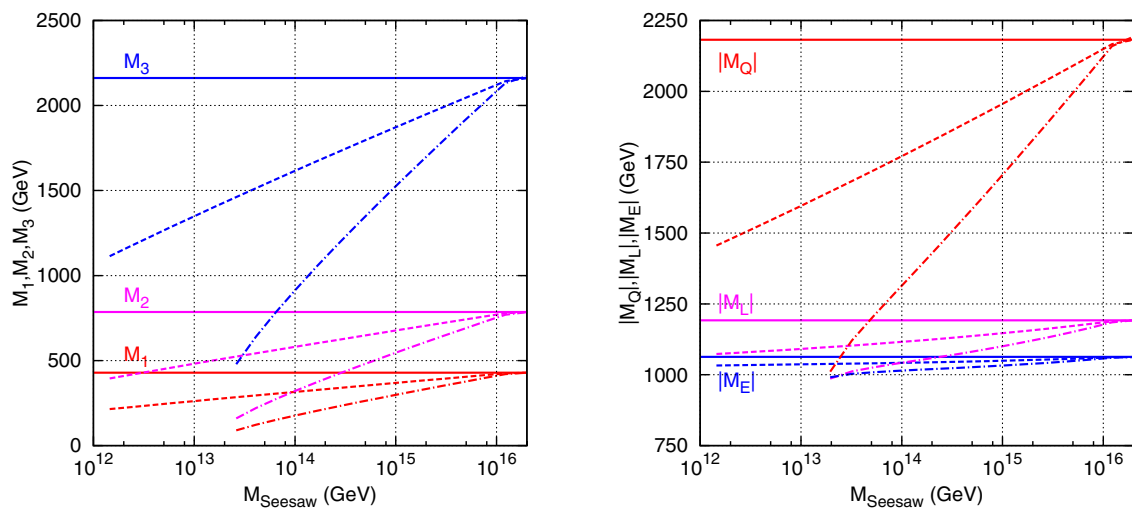

FIG. 1 (color online). Mass parameters at $Q = 1$ TeV versus the seesaw scale for fixed high scale parameters $m_0 = M_{1/2} = 1$ TeV, $A_0 = 0$, $\tan\beta = 10$, and $\mu > 0$. The full lines correspond to seesaw type-I, the dashed ones to type-II, and the dash-dotted ones to type-III. In all cases, a degenerate spectrum of the seesaw particles has been assumed.
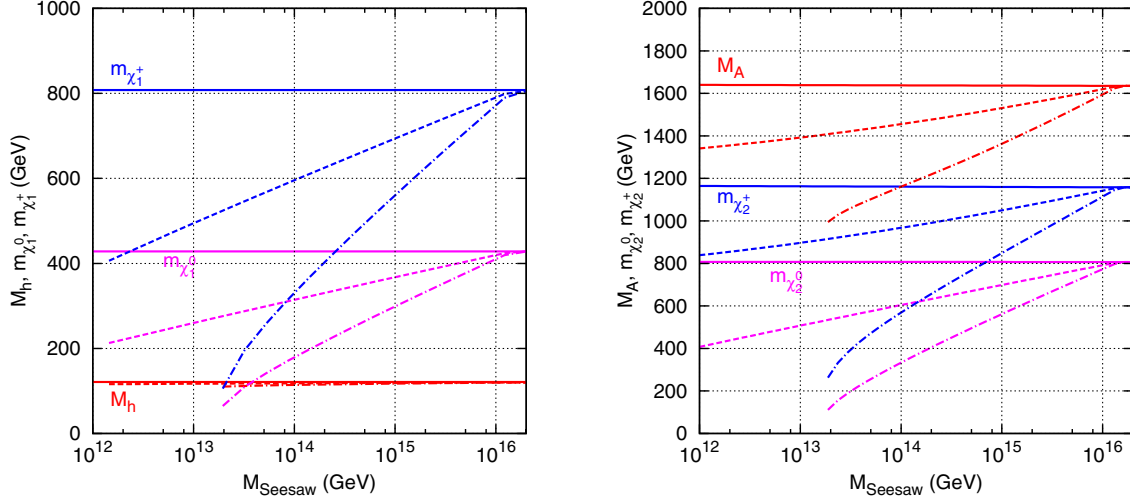
FIG. 2 (color online).   Example of spectra at $Q = 1$ TeV versus the seesaw scale for fixed high scale parameters $m_0 = M_{1/2} = 1$ TeV, $\tan\beta = 10$, and $\mu > 0$. On left panel M_h, $m_{\tilde\chi_1^0}$, $m_{\tilde\chi_1^+}$, while on the right panel we have M_A, $m_{\chi_2^0}$, $m_{\tilde\chi_2^+}$. The line codes are as in Fig. 1.

missing members of the gauge fields and the Higgs fields responsible for the breaking of the GUT group [53]. A second reason why the deviations between the leading-log calculation, the case of 1-loop and 2-loop RGEs gets larger for smaller seesaw scale is that the increase of the beta coefficients implies larger values of the gauge couplings at the GUT scale. This implies that one reaches a Landau pole for sufficiently low values of the seesaw scale. As an example, we show in Fig. 5 the value of the gauge coupling at $M_{\rm GUT} = 2 \times 10^{16}$ GeV as a function of the seesaw scale for type-II with a pair of **15** plets (black lines) and type-III with three degenerate **24** plets (green lines). In both cases, the 2-loop RGEs imply a larger gauge coupling for a fixed

seesaw scale. One sees that in case of type-II (type-III) in principle one could reach a seesaw scale of about 10^8 GeV (10^{13} GeV). However, we believe that we can no longer trust even the 2-loop calculation for such large values of the g_i, as the neglected higher order terms become more and more important. Especially, we should not trust the ''turn-over'' of the invariants in Fig. 4 for very low values of the seesaw scale, since the numerical calculation at these points is already very close to breaking down.

We would also like to mention that, in the numerical calculation we find very often that one of the scalar masses squared, in particular, staus and/or sbottoms, gets large negative values already for values of the seesaw scale larger than the Landau pole and thus we can not go to values of the seesaw scale as low as the examples shown in Fig. 4 in many SUSY points.
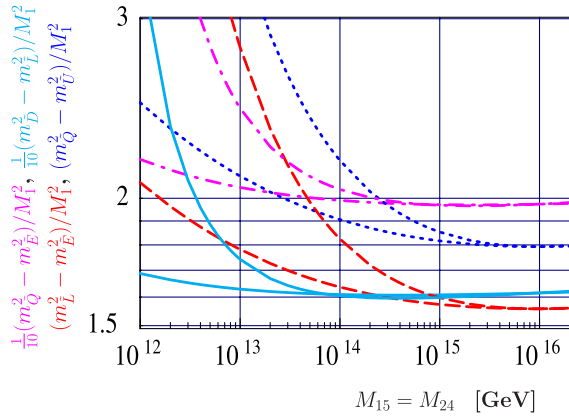
E. Lepton flavour violation in the slepton sector

From a one-step integration of the RGEs, one gets, assuming mSUGRA boundary conditions, a first rough estimate for the lepton flavour violating entries in the slepton mass parameters:

$$m_{L,ij}^2 \simeq -\frac{a_k}{8\pi^2}(3m_0^2 + A_0^2)(Y_N^{k,\dagger} L Y_N^k)_{ij}, \qquad (20)$$

FIG. 3 (color online).   Four different ''invariant'' combinations of soft masses versus the mass of the **15** plet *or* **24** plet, $M_{15} = M_{24}$. The plot assumes that the Yukawa couplings are negligibly small. The calculation is at 1-loop order in the leading-log approximation. The lines running faster up towards smaller M are for type-III seesaw; the values for type-II seesaw are shown for comparison.

$$A_{l,ij} \simeq -a_k \frac{3}{16\pi^2} A_0 (Y_e Y_N^{k,\dagger} L Y_N^k)_{ij}, \qquad (21)$$

for $i \neq j$ in the basis, where Y_e is diagonal, $L_{ij} = \ln(M_{\rm GUT}/M_i)\delta_{ij}$, and Y_N^k is the additional Yukawa coupling of the type-k seesaw at $M_{\rm GUT}$ ($k = $ I, II, III). We obtain

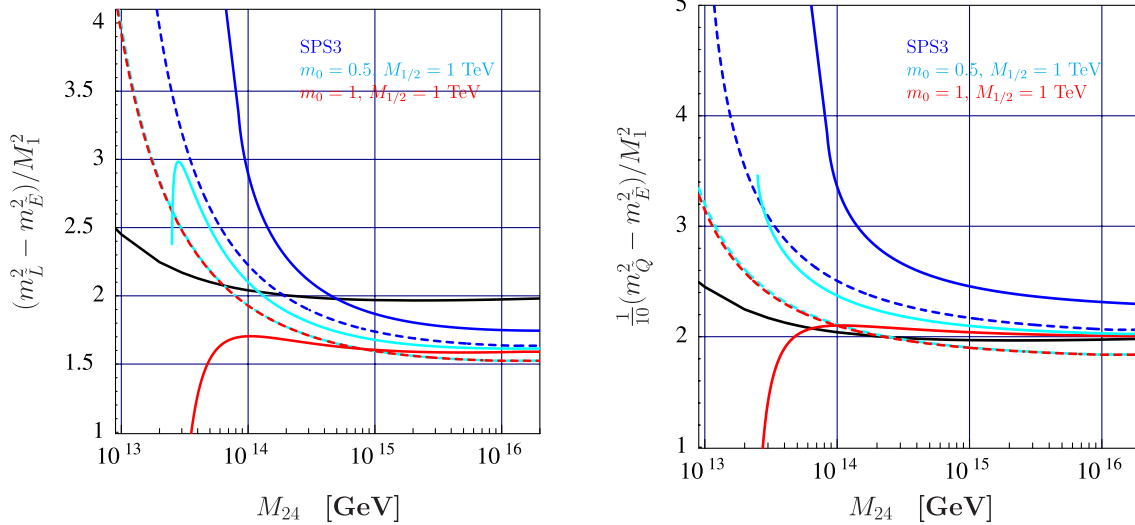$$a_I = 1, \qquad a_{II} = 6 \quad \text{and} \quad a_{III} = \frac{9}{5}. \qquad (22)$$

FIG. 4 (color online).   The limits of the invariants in seesaw type-III models. Left: $(m_L^2 - m_E^2)/M_1^2$; right: $(m_Q^2 - m_E^2)/M_1^2$. The blue lines are for SPS3, the light blue one for $m_0 = 500$ GeV and $M_{1/2} = 1$ TeV, and the red one for $m_0 = M_{1/2} = 1$ TeV; full (dashed) lines are 2-loop (1-loop) results. The black line is the analytical approximation, for comparison.

Note, that in case of the type-II the matrix L is degenerate and thus can be factored out. All models have in common that they predict negligible flavour violation for the right-sleptons

$$m_{E,ij}^2 \simeq 0. \qquad (23)$$

We know that these approximations work well only in case of the type-I models. Nevertheless, they give a rough idea on the relative size one has to expect for the rare lepton decays $l_i \rightarrow l_j \gamma$, which very roughly scale like

FIG. 5 (color online).   Values of the gauge coupling at $M_{\mathrm{GUT}} = 2 \times 10^{16}$ GeV as a function of the seesaw scale, black lines seesaw type-II and green lines seesaw type-III with three **24** plets with degenerate mass spectrum; full (dashed) lines are 2-loop (1-loop) results. For the calculation of the electroweak threshold, the spectrum corresponds to $m_0 = M_{1/2} = 1$ TeV, $A_0 = 0$, $\tan\beta = 10$, and $\mu > 0$.

$$\mathrm{Br}\,(l_i \rightarrow l_j\gamma) \propto \alpha^3 m_{l_i}^5 \frac{|m_{L,ij}^2|^2}{\tilde{m}^8} \tan^2\beta, \qquad (24)$$

where $\tilde{m}$ is the average of the SUSY masses involved in the loops. Note that for a given set of high scale parameters both the different size of the flavour mixing entries and the changed mass spectrum play a role.

III. NUMERICAL RESULTS

In this section, we present our numerical calculations. All results presented below have been obtained with the lepton flavour violating version of the program package SPHENO [54,55]. The RGEs of the seesaw II and seesaw III models have been calculated with SARAH [43–45]. All seesaw parameters are defined at M_{GUT}, and as mentioned in the previous section we require for models of type-II the boundary condition $Y_Z = Y_S = Y_T$ and $M_Z = M_S = M_T$ and in case of type-III models $Y_N = Y_B = Y_W$ and $M_B = M_G = M_W = M_X$. We evolve the RGEs to the scale(s) corresponding to the GUT-scale values of the masses of the heavy particles. The RGE evolution implies also a splitting of the heavy masses. We therefore add at the corresponding scale the threshold effects due to the heavy particles to account for the different masses. In case of type-III models, off-diagonal elements are induced in the mass matrices. This implies that one has to go the corresponding mass eigenbasis before calculating the threshold effects. We use 2-loop RGEs everywhere except stated otherwise. In the Appendix, we give the necessary ingredients on how to obtain them in the seesaw type-II and III models. The analogous anomalous dimensions for the type-I model can be found in [56].

Unless mentioned otherwise, we fit neutrino mass squared differences to their best fit values [5] and the
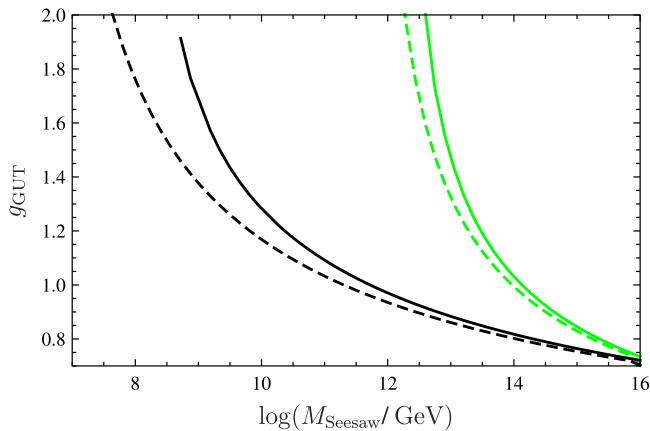
angles to tri-bi-maximal (TBM) values [57]. Our numerical procedure is as follows. Inverting the seesaw equation, see Eqs. (12) and (18), one can get a first guess of the Yukawa couplings for any fixed values of the light neutrino masses (and angles) as a function of the corresponding triplet mass for any fixed value of the couplings. This first guess will not give the correct Yukawa couplings, since the neutrino masses and mixing angles are measured at low energy, whereas for the calculation of m_ν we need to insert the parameters at the high energy scale. However, we can use this first guess to run numerically the RGEs to obtain the exact neutrino masses and angles (at low energies) for these input parameters. The difference between the results obtained numerically and the input numbers can then be minimized in a simple iterative procedure until convergence is achieved. As long as neutrino Yukawas are $\forall Y_{ij} < 1$, we reach convergence in a few steps. However, in seesaw type-II and type-III the Yukawas run stronger than in seesaw type-I, so our initial guess can deviate sizably from the correct Yukawas, implying in general also more iterations until full convergence is reached. Since neutrino data requires at least one neutrino mass to be larger than about 0.05 eV, we do not find any solutions for $M_T \gtrsim \lambda_2 \times 10^{15}$ GeV and $M_{24} \gtrsim 8 \times 10^{14}$ GeV, respectively. In the latter case, we have assumed that all 24 plets have similar masses. For sake of completeness, we note that one can also satisfy all neutrino data by giving one of the 24 plets a large mass in the order of $M_{\rm GUT}$ or larger having a model with effectively only two 24 plets.

A. Lepton flavour violation

We have seen in Eq. (24) that rates for the lepton flavour violating decays of μ and τ scale like the LFV entries in the slepton mass squared matrix squared and inverse to the overall SUSY mass to the power eight. From this one

immediately concludes the rates for the rare lepton decays are in general larger in seesaw models of type-II and III than in type-I models for fixed SUSY masses and seesaw scales except if one arranges for special cancellations.

Comparing the type-II with the type-III model, one finds that LFV decays are larger for type-III, as shown for the case of $\mu \to e\gamma$ in Fig. 6. From Eqs. (21) and (22), however, one would expect that type-II should have larger LFV. Numerically, we find the opposite for two reasons: (i) $\mathrm{Br}(l_i \to l_j\gamma)$ strongly depends on the SUSY masses, see Eq. (24) and type-III has a lighter spectrum than type-II (for the same mSUGRA input parameters). And (ii) 2-loop effects are very important in type-III, due to the large coefficients, in general, leading to large flavor violating soft SUSY-breaking parameters.

In Fig. 6, we compare $\mathrm{Br}(l_i \to l_j\gamma)$ for the three seesaw models taking degenerate seesaw spectra in case of type-I and type-III. Note that in case of seesaw type-III we can only show a relatively short interval for the seesaw scale which is mainly due to two reasons: (i) For scales below approximately 10^{13} GeV the gauge couplings get large at $M_{\rm GUT}$ as a consequence of the large beta functions and, thus, perturbation theory breaks down. (ii) One encounters negative mass squares for the scalars, in particular, for the lighter stau and/or lighter sbottom. The latter point is also the reason why the possible range is larger in case of the larger soft SUSY-breaking parameters.

The values for $\mathrm{Br}(\mu \to e\gamma)$ in Fig. 6 are larger than the current experimental bound [58], so one might worry if in case of type-III models only SUSY spectra beyond the reach of the LHC are allowed. (Note that even for the examples shown the masses of the sfermions are already in the range of several hundred GeVs as can be seen from Table I.) Indeed, we find that by putting generic Yukawa couplings which are able to explain neutrino data one needs a heavy spectrum to be consistent with bounds on
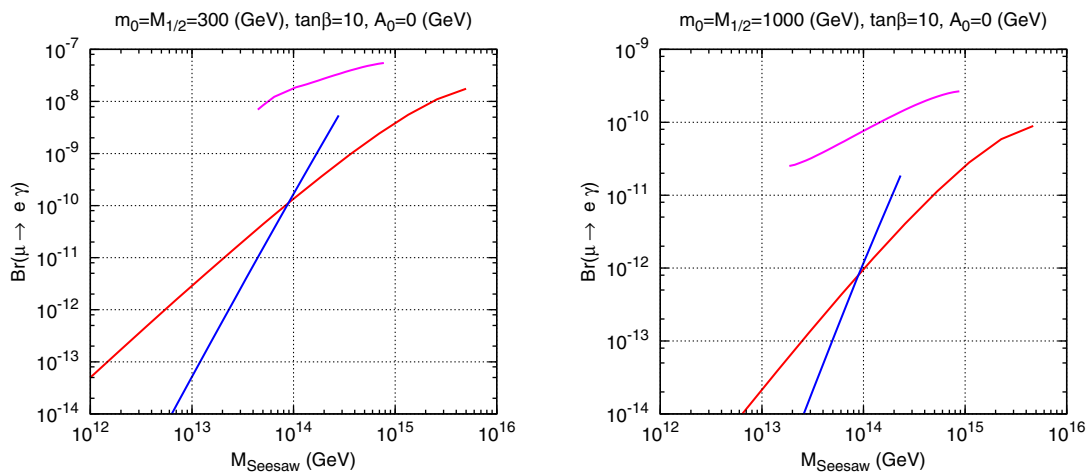

FIG. 6 (color online). $\mathrm{Br}(\mu \to e\gamma)$ as a function of the seesaw scale for seesaw type-I (red line), seesaw type-II (blue line), and seesaw type-III (magenta line). In case of type-I and type-III, a degenerate spectrum has been assumed. On the left panel $m_0 = m_{1/2} = 300$ (GeV); on the right panel $m_0 = m_{1/2} = 1000$ (GeV). In both cases, we take $\tan\beta = 10$, $A_0 = 0$, and $\mu > 0$.

TABLE I. Examples masses in GeV for $M_{1/2} = 1000$ GeV, $\tan\beta = 10$, $A_0 = 0$ GeV, and $\mu > 0$, for seesaw type-III for a degenerate seesaw spectrum with $M_{24} = 10^{14}$ GeV.

m_0	$m_{\tilde{\chi}_1^0}$	$m_{\tilde{\chi}_1^+}$	$m_{\tilde{\chi}_2^+}$	$m_{\tilde{g}}$	$m_{\tilde{\tau}_1}$	$m_{\tilde{e}_R}$	$m_{\tilde{e}_L}$	$m_{\tilde{t}_1}$
500	178	333	617	1029	535	543	600	772
1000	180	338	642	1057	1008	1020	1043	925

the rare lepton decays. However, this is strictly true only for the TBM angles and $R = \mathbf{1}$. Accidental cancellations due to different contributions to the flavor violating soft masses and thus to the rare lepton decays are possible in type-III (and in type-I). As an example, we show in Fig. 7 $\mathrm{Br}(\mu \to e\gamma)$ as a function of the reactor angle s_{13}^2 for different values of the Dirac phase δ. For comparison, we also show the calculation for a type-I model. For $\delta = \pi$ there is a range of s_{13}^2 where this branching ratio is below the experimental constraint.

At first glance, this seems to require some fine-tuning of the underlying parameters. However, one can look at this from a different perspective: Assume that the MEG Collaboration has found a nonvanishing value for $\mathrm{Br}(\mu \to e\gamma)$ and from LHC data one has found that the spectrum is consistent with the type-III seesaw model. For a fixed R matrix, e.g. $R = \mathbf{1}$, one would obtain in this case a relation between s_{13}^2 and M_{24}. This can be exploited to put a bound on M_{24} or even to determine it depending on the outcome of measurements of reactor angle and, thus, the model assumptions can be tested. In Fig. 8, we show the corresponding rare tau decays. Note that also for

$\tau \to e\gamma$ such a cancellation exists in principle but the corresponding range is excluded by $\mu \to e\gamma$. In contrast, $\tau \to \mu\gamma$ is insensitive to the reactor angle and should be measurable in the near future.

Up to now, we have assumed that the seesaw spectrum is nearly degenerate, which is of course a strong assumption. We show in Fig. 9 two examples where we keep in each case two masses fixed and vary the third one. Note, that in contrast to SUSY particles the indices of the heavy particles are generation indices and do not correspond to a particular mass ordering, e.g. M_{R_2} corresponds to the 'solar neutrino scale'' and M_{R_3} to the "atmospheric neutrino scale''. In case that the mass of the first generation state is varied, e.g. the left plot of this figure, one finds a decrease of the branching ratios with increasing seesaw mass M_{R_1}. This is mainly caused by an increase of the SUSY spectrum, while at the same time neutrino physics is only affected mildly, requiring only a light increase of the corresponding Yukawa couplings to obtain the correct neutrino masses. If, on the other hand, the mass M_{R_3} of the third generation seesaw particles is increased one needs also a sizable increase of the Yukawa couplings to obtain the correct neutrino mass difference squared for the atmospheric sector. This leads to the observed behavior that the branching ratios for $\tau \to \mu\gamma$ and $\tau \to 3\mu$ increases while the other ones decrease.

B. Dark matter

The changes in the spectrum induced by the new heavy states also impact on the predictions with respect to the relic density which we have calculated using the program MICROMEGAS [59]. As is well-known, within mSUGRA there are 4 regions in parameter space, in which the constraint from dark matter can be satisfied. These are (i) the bulk region; (ii) the stau coannihilation region; (iii) the focus point line and (iv) the Higgs-funnel. Below, we will show usually the range of Ωh^2 allowed at 3σ according to [58]

$$0.081 \leq \Omega h^2 \leq 0.129. \qquad (25)$$

In particular, the coannihilation region is very sensitive to the difference between the masses of the lightest stau and the lightest neutralino. In Fig. 10, we observe that this difference depends strongly on the seesaw scale in both models. For a fixed $M_{1/2}$ and m_0 lowering the seesaw scale increases this mass difference, which then leads to a larger
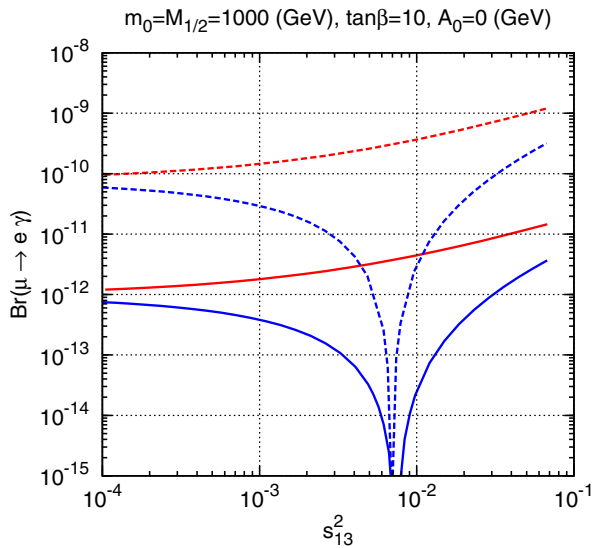

FIG. 7 (color online). $\mathrm{Br}(\mu \to e\gamma)$ versus s_{13}^2 for $m_0 = M_{1/2} = 1000$ GeV, $\tan\beta = 10$, $A_0 = 0$ GeV, and $\mu > 0$, for seesaw type-I (solid lines) and seesaw type-III (dashed lines), for $M_{\mathrm{Seesaw}} = 10^{14}$ GeV. The curves shown are for 2 values of the Dirac phase: $\delta = 0$ (red) and $\delta = \pi$ (blue), both for normal hierarchy.
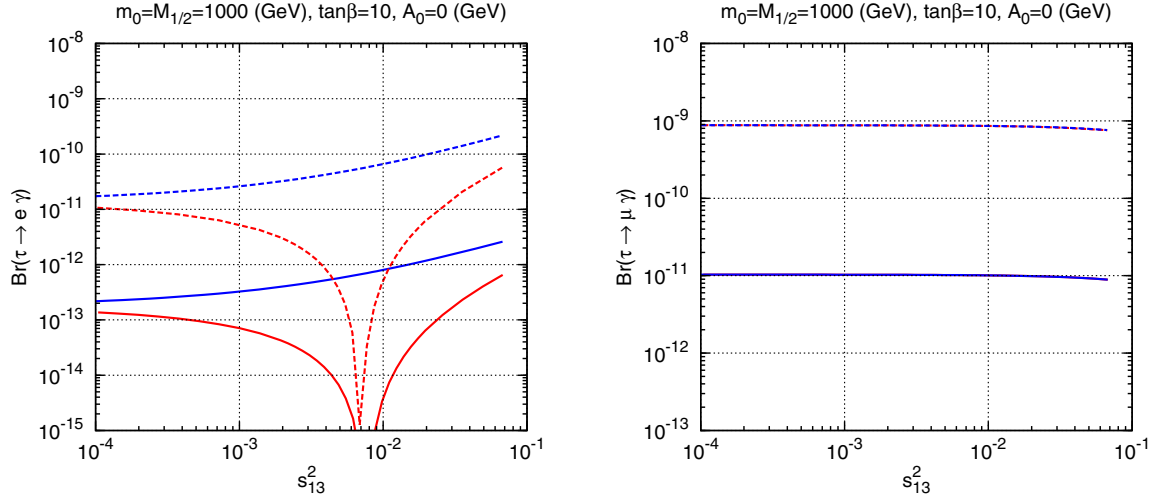
FIG. 8 (color online). $\mathrm{Br}(\tau \to e\gamma)$ versus s_{13}^2 (left) and $\mathrm{Br}(\tau \to \mu\gamma)$ versus s_{13}^2 (right) for $m_0 = M_{1/2} = 1000$ GeV, $\tan\beta = 10$, $A_0 = 0$ GeV, and $\mu > 0$, for seesaw type-I (solid lines) and seesaw type-III (dashed lines), for $M_{\mathrm{Seesaw}} = 10^{14}$ GeV. The curves shown are for $\delta = 0$ (red) and $\delta = \pi$ (blue) for normal hierarchy.

calculated Ωh^2. To compensate for this effect, one needs to lower m_0, with the value depending on the seesaw scale chosen. For certain seesaw scales then m_0 needs to be lowered below $m_0 = 0$ and the coannihilation region disappears. In this region of parameter space, both models behave in a qualitatively similar way. However, recall that spectra run faster towards smaller masses in seesaw type-III.

Also the focus point region is very sensitive to the precise values of the input parameters. The focus point region appears in mSUGRA for large values of m_0

and small/moderate values of $M_{1/2}$ of the order of $\mathcal{O}(100)$ GeV, the exact value depending on m_0. This can be seen in Figs. 11 and 12, where we show $m_{\tilde\chi_1^0}$, the Higgsino content $|N_{13}|^2 + |N_{14}|^2$, and the corresponding Ωh^2 as a function of m_0 for a fixed seesaw scale $M_{T,W} = 10^{14}$ GeV, $A_0 = 0$, $\tan\beta = 10$, $\mu > 0$, and various values of $M_{1/2}$. Note that we take different values of $M_{1/2}$ for the two models in such a way that we obtain similar values for $m_{\tilde\chi_1^0}$. We find that both models behave differently in this region of parameter space, e.g. the Higgsino content $|N_{13}|^2 + |N_{14}|^2$ decreases (increases) with increasing
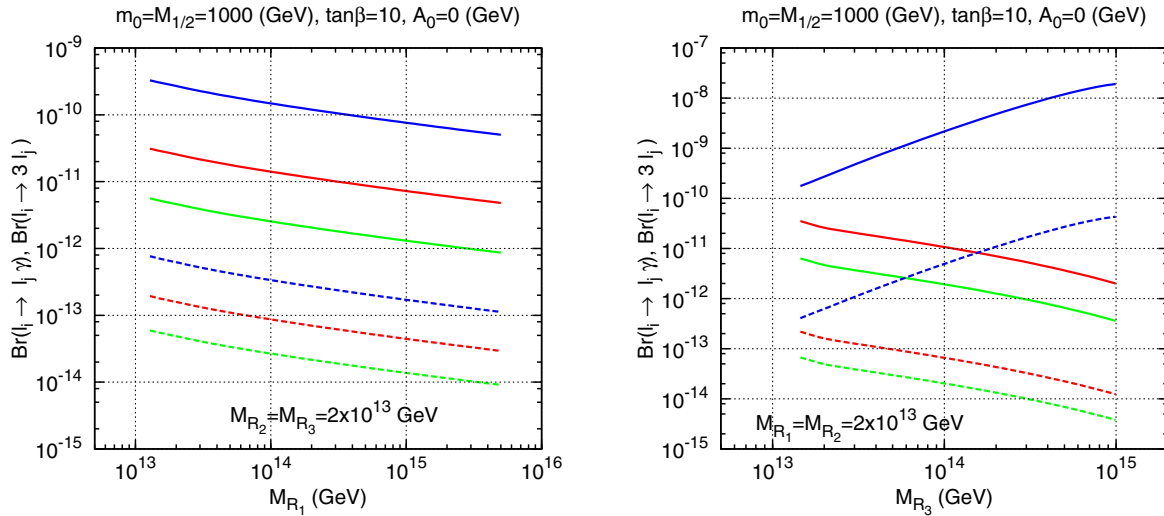

FIG. 9 (color online). Branching ratios for $l_i \to l_j \gamma$ (solid lines) and $l_i \to 3l_j$ (dashed lines) versus the seesaw scale for $\tan\beta = 10$, $\mu > 0$, $A_O = 0$ GeV, $M_{1/2} = m_0 = 1000$ GeV. On the left panel, we scan on M_{R_1} with $M_{R_2} = M_{R_3} = 2 \times 10^{13}$ GeV, while on the right panel we scan on M_{R_3} with $M_{R_1} = M_{R_2} = 2 \times 10^{13}$ GeV. The color code is red for $\mu \to e\gamma$ or $\mu \to 3e$, blue for $\tau \to \mu\gamma$ or $\tau \to 3\mu$, and green for $\tau \to e\gamma$ or $\tau \to 3e$.
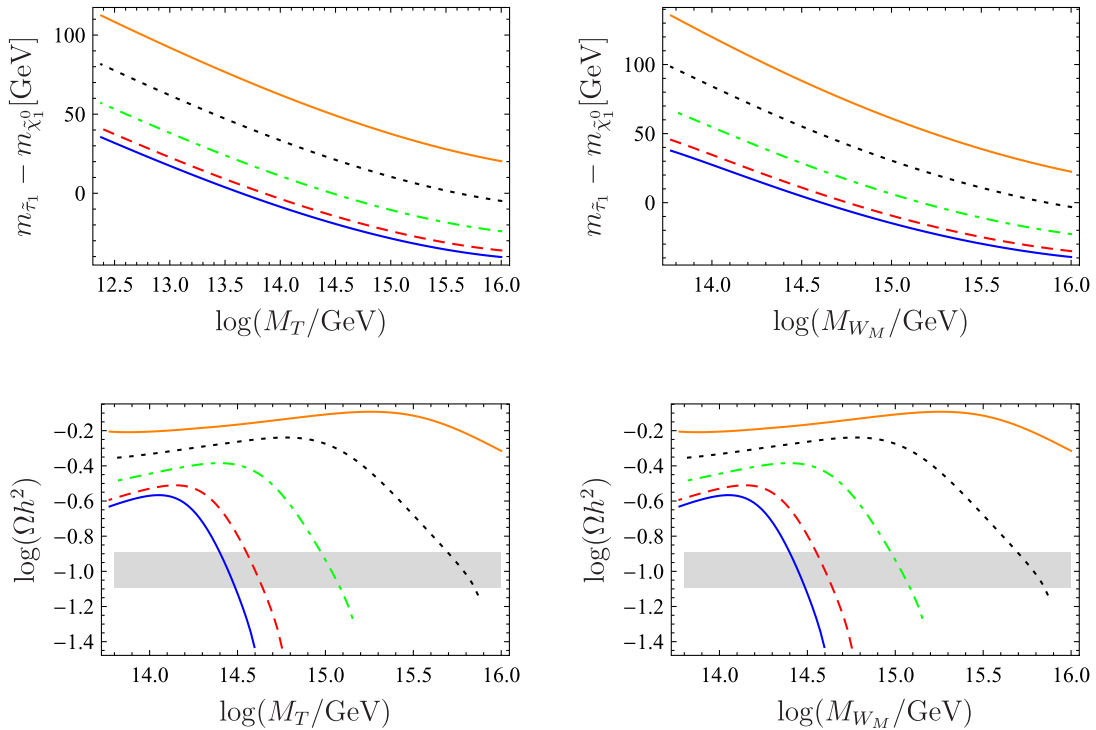
FIG. 10 (color online). Difference between the masses and the lightest stau and the lightest neutralino (upper row) as well as the corresponding Ωh^2 (lower row) as a function of the seesaw scale. The left (right) plots are for seesaw type-II (III). A degenerate seesaw spectrum has been assumed in case of seesaw type-III. $M_{1/2} = 800$ GeV, $A_0 = 0$, $\tan\beta = 10$, and $\mu > 0$. The lines correspond to full blue line $m_0 = 0$, red dashed line $m_0 = 50$ GeV, green dashed dotted line $m_0 = 100$ GeV, black dashed line $m_0 = 150$ GeV, and orange full line $m_0 = 200$ GeV. The gray band shows the preferred range according to Eq. (25).

values m_0 for seesaw type-II (type-III). However, also for type-II, the Higgsino content increases for increasing m_0 once we reach the multi-TeV range, but we did not get correct electroweak symmetry breaking in case of multi-TeV values for m_0 in case of type-III models. The increased Higgsino content of the lightest neutralino leads to on increase (decrease) of its couplings to the Z boson and the light Higgs boson (to sfermions) resulting in the observed dependence of Ωh^2 for m_0 close to the 1-TeV region.

With these observations, it is clear that the Dark Matter (DM) allowed regions will be shifted in the m_0-$M_{1/2}$ plane compared to the usual mSUGRA expectations. We fix in the following $m_{\text{top}} = 171.2$ GeV, $\tan\beta = 10$, $A_0 = 0$, and $\mu > 0$ as well as the seesaw scale to 10^{14} GeV. For comparison, we show in Fig. 13 the usual mSUGRA case without any heavy intermediate particles (left plot), as well as the case of a seesaw type-I scenario (right plot). The blue bands show the 3σ range according to [58], and we see the three usual regions: the stau coannihilation with
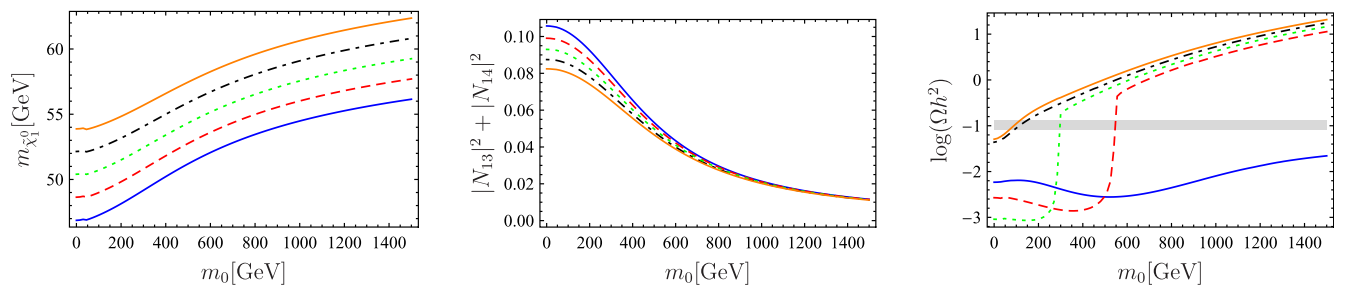

FIG. 11 (color online). Mass of the lightest neutralino (left plot), its Higgsino content (middle plot), and the corresponding Ωh^2 (right plot) as a function of m_0 for a seesaw type-II model with $M_T = 10^{14}$ GeV, $m_{\text{top}} = 171.2$ GeV, $A_0 = 0$, $\tan\beta = 10$, and $\mu > 0$. The lines correspond to full blue line $M_{1/2} = 195$ GeV, red dashed line $M_{1/2} = 200$ GeV, green dashed dotted line $M_{1/2} = 205$ GeV, black dashed line $M_{1/2} = 210$ GeV, and orange full line $M_{1/2} = 215$ GeV. The gray band shows the range Eq. (25).
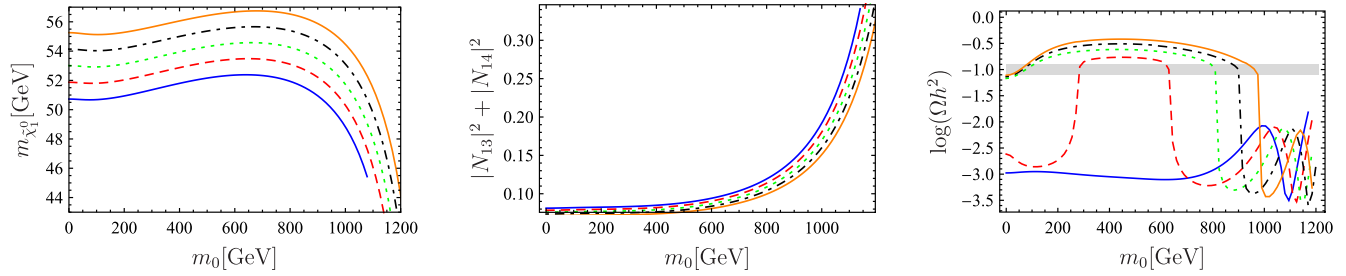
FIG. 12 (color online).   Mass of the lightest neutralino (left plot), its Higgsino content (middle plot), and the corresponding Ωh^2 (right plot) as a function of m_0 for a seesaw type-III model with a degenerate seesaw scale $M_W = 10^{14}$ GeV, $m_{\text{top}} = 171.2$ GeV, $A_0 = 0$, $\tan\beta = 10$, and $\mu > 0$. The lines correspond to full blue line $M_{1/2} = 400$ GeV, red dashed line $M_{1/2} = 405$ GeV, green dashed dotted line $M_{1/2} = 410$ GeV, black dashed line $M_{1/2} = 415$ GeV, and orange full line $M_{1/2} = 420$ GeV. The gray band shows the range Eq. (25).

a lighter stau mass close to the LSP mass for $M_{1/2} \lesssim 300$ GeV, the bulk region for moderate values of $M_{1/2}$, and m_0 resulting in small sfermion masses as well as the focus point region for $M_{1/2} \simeq 170$ GeV and large values of m_0. In addition, we show the lines corresponding to $M_h = 110$ GeV and 114 GeV. Note that the theoretical uncertainty on M_h is still of the order of 3–5 GeV [60,61]. Moreover, the value of the Higgs boson mass also depends strongly on A_0, and, in particular, for negative values of A_0, one can easily increase the value of M_h, while the DM allowed regions hardly change.

The part of parameter space most affected is the one at large m_0. Since in mSUGRA μ is calculated from the requirement of correct electroweak symmetry breaking, μ changes rapidly in this region. With the Higgsino content in the lightest neutralino changing rapidly as a func-

tion of μ, this region is then very sensitive to any changes of parameters. Since the Y_ν also impacts on the running of the Higgs mass parameters and thus slightly affects the value predicted for μ, some small changes are found relative to mSUGRA here. Note, however, that this region is highly constrained by the lower bound on the lightest chargino mass of the order of 103 GeV [62].

In case of the other two seesaw models, the shift of the allowed regions is much more pronounced, as discussed above. In Figs. 14 and 15, we show two regions for type-II (left plot) and type-III (right plot) and two different values for A_0. As claimed above, the Higgs mass bounds gets shifted significantly, while the DM allowed regions are hardly affected. As expected, the effects are much more pronounced in case of type-III as the effects of the heavy particles on the spectrum are much stronger. Note, that in
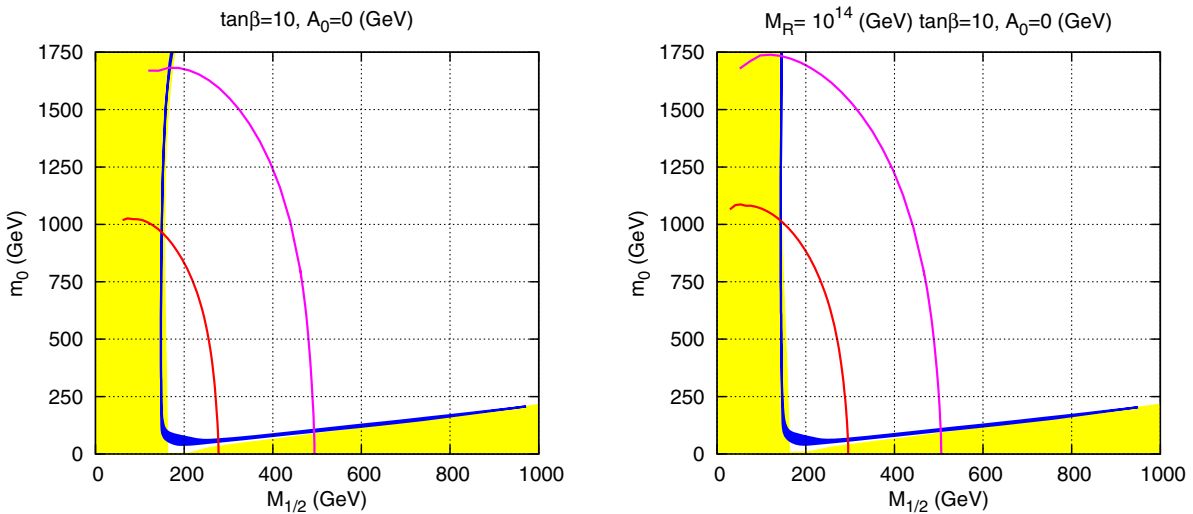

FIG. 13 (color online).   Dark matter allowed region (in blue) for mSUGRA (left panel) and for type-I seesaw (right panel). The parameters are $\tan\beta = 10$, $A_0 = 0$, $\mu > 0$, and $M_T = 10^{14}$ GeV for $m_{\text{top}} = 171.2$ GeV. Also shown (in yellow) are the regions excluded by LEP (small values of $M_{1/2}$) and by LSP constraint (small values of m_0). Also shown are the Higgs boson mass curves for $M_h = 110$ GeV (in red) and for $M_h = 114.4$ GeV (in magenta).
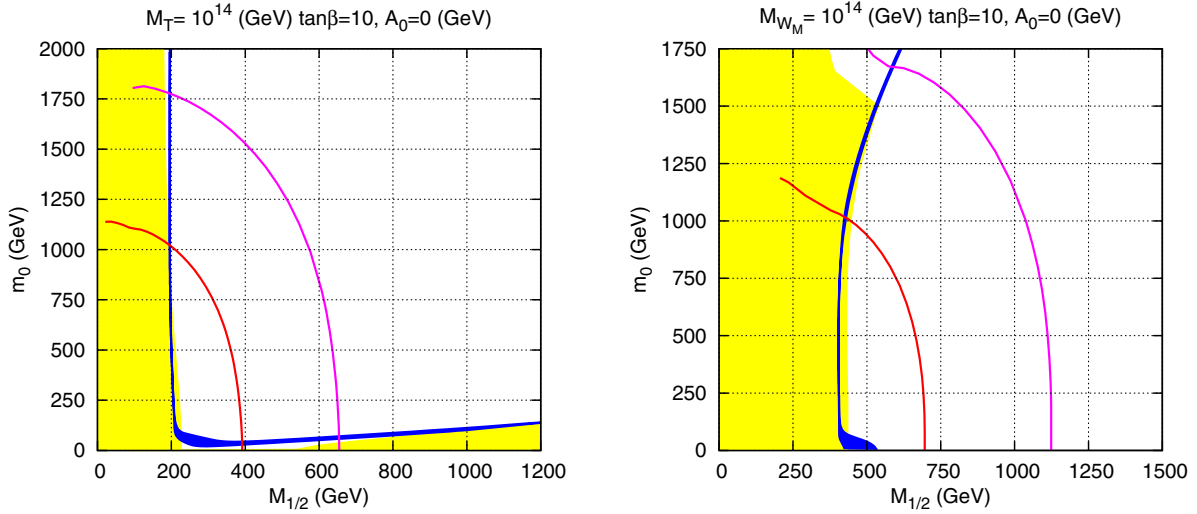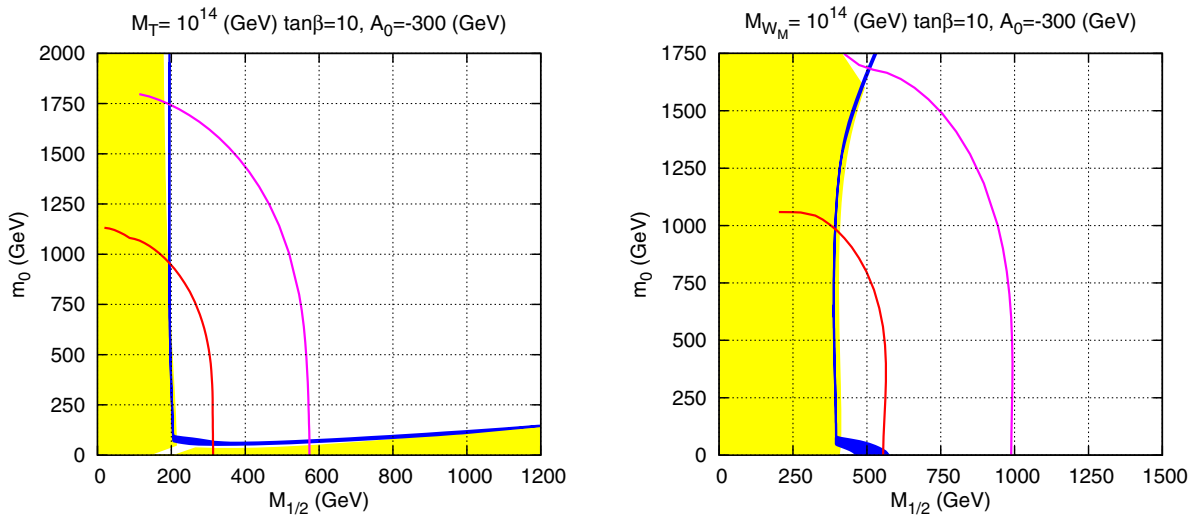
FIG. 14 (color online).   Like in Fig. 13 but for seesaw type-II (left panel) and type-III (right panel).

FIG. 15 (color online).   Like in Fig. 14 but for $A_0 = -300$. Seesaw type-II (left panel) and type-III (right panel).

particular, the bending of the allowed region for large m_0 is due to the changed Higgsino content as discussed in case of Figs. 11 and 12. Moreover, the case of stau coannihilation is not viable anymore in case of the type-III model already for this value of the seesaw scale. For completeness, we mention that for the type-II the stau coannihilation region disappears (below $M_{1/2} = 1500$ GeV) for $M_T \lesssim 10^{13}$ GeV. For completeness, we note that the results here differ slightly from the ones of our previous work [42] because (i) of the corrections of the 1-loop RGEs of Ref. [14] by [47] and (ii) the complete set of 2-loop RGEs are now used.

In the case of large $\tan\beta$, an additional region, usually called the Higgs funnel, opens up. This region is characterized by $M_A \simeq 2m_{\tilde{\chi}_1^0}$. Also, here the regions get shifted compared to usual mSUGRA scenario. However, this re-

gion is very sensitive to higher order corrections, and therefore it is quite important to use full 2-loop RGEs as can be seen in Fig. 16. We have again fixed $A_0 = 0$, $\mu > 0$, $m_{\text{top}} = 171.2$ GeV, and the seesaw scale to 10^{14} GeV, with a degenerate spectrum in case of the type-III model. The main reason for the observed and rather surprisingly large differences between the different calculations is that the 2-loop contributions decrease the neutralino mass compared to the 1-loop case while at the same time increasing M_A. For example, in case of seesaw II and for fixed values of $m_0 = M_{1/2} = 1500$ GeV, we get in case of 1-loop RGEs $m_{\tilde{\chi}_1^0} = 560$ GeV, $M_A = 1090$ GeV and in case of 2-loop RGEs $m_{\tilde{\chi}_1^0} = 498$ GeV, $M_A = 1100$ GeV. For completeness, we note that this region is also very sensitive to input values for m_t and m_b [42].
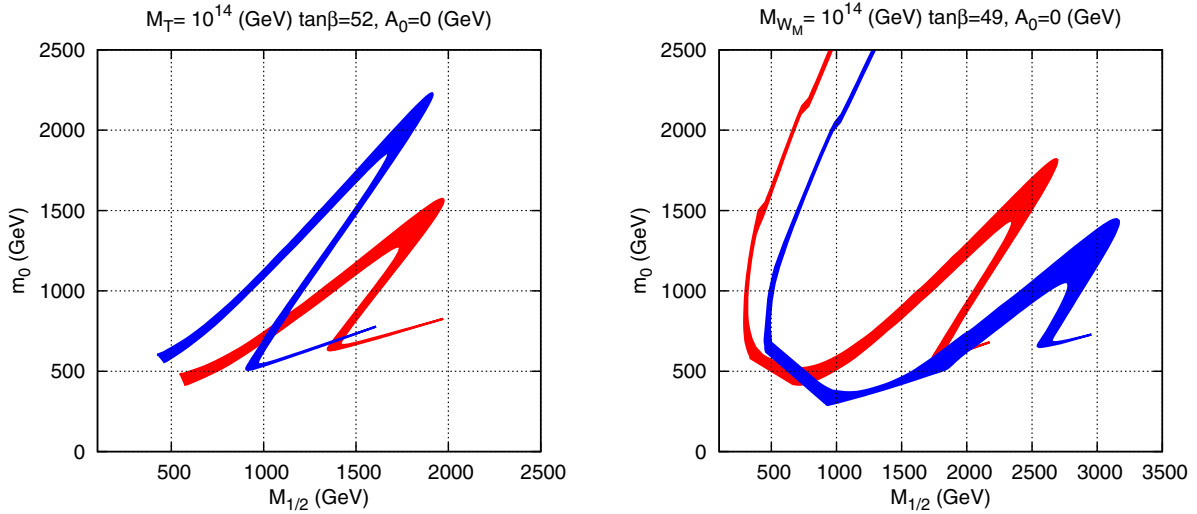
FIG. 16 (color online).   Comparison between using 1-loop (red) or 2-loop (blue) RGEs on the dark matter allowed region for type-II (left panel) and type-III (right panel). The parameters are $A_0 = 0$, $\mu > 0$ and $M_{\text{Seesaw}} = 10^{14}$ GeV, $m_{\text{top}} = 171.2$ GeV and $\tan\beta = 52$ for type-II and $\tan\beta = 49$ for type-III.

IV. CONCLUSIONS AND OUTLOOK

To summarize, we have investigated in detail a supersymmetric version of a seesaw model of type-III and compared it to seesaw models of type-I and type-II. In case of type-II and type-III models, we have embedded the $SU(2)$ triplets in the corresponding $SU(5)$ representations to maintain gauge coupling unification, e.g. **15** plets in case of type-II and **24** plets in case of type-III models. For definiteness, we have assumed mSUGRA boundary conditions for the soft SUSY-breaking parameters.

The additional heavy charged states lead to changes in the beta functions and, thus, also in the running of the SUSY mass parameters. We have calculated the soft masses as a function of the seesaw parameters. As discussed in some detail, there are certain combinations of soft masses, which are approximately constants over large regions of mSUGRA space. These invariants contain indirect information about the seesaw scale assuming the type of seesaw model. In certain parts of the parameter space, e.g. for low seesaw scales, one might even be able to exclude certain seesaw models by combining mass measurements at the LHC with the mSUGRA paradigm. We note that using 2-loop RGEs will be crucial to obtain reliable results.

The changes in the spectrum lead obviously to changes in the phenomenology. We have calculated lepton flavour violating observables, such as $\text{Br}(l_i \rightarrow l_j + \gamma)$. We find that for fixed (degenerate) seesaw scale these branching ratios are in general largest for type-III models followed by type-II and type-I. This is a consequence of the fact that for a given set of mSUGRA parameters the spectrum in type-III is lighter than for type-II models, which is again lighter than in type-I models. However, the difference in the predictions of type-II and type-III is somewhat smaller than expected from these considerations because in type-II models the flavour violating entries are larger compared to the case of type-III models.

We also investigated the predictions for the relic density Ωh^2 in the type-III model and compared them with the other models. We find the usual four regions in the mSUGRA parameter space, but of course they are shifted due to the changes in the spectrum. It has been found that, in particular, in case of the Higgs funnel the use of 2-loop RGEs is crucial to identify the correct allowed region. Last, but not least, we note that for low seesaw scales the coannihilation region vanishes for both, the type-II and the type-III models, as the required mass difference between the lightest neutralino and the stau cannot be obtained anymore.

APPENDIX: RGES FOR THE SEESAW TYPE-II AND SEESAW TYPE-III MODELS AT 2-LOOP

In the Appendix, we collect the beta coefficients for the gauge couplings as well as anomalous dimensions of the superfields, which are the ingredients to calculate the 2-loop RGEs for both, the seesaw type-II and type-III, models using the procedure given in [63] based on the spurion formalism [64]. The complete set of RGEs for both models at 2-loop is also given online [65]. In the following, we briefly summarize the basic ideas of this calculation for completeness.

For a general $N = 1$ supersymmetric gauge theory with superpotential

$$W(\phi) = \frac{1}{2}\mu^{ij}\phi_i\phi_j + \frac{1}{6}Y^{ijk}\phi_i\phi_j\phi_k \qquad (A1)$$

the soft SUSY-breaking scalar terms are given by

$$V_{\text{soft}} = \left(\frac{1}{2}b^{ij}\phi_i\phi_j + \frac{1}{6}h^{ijk}\phi_i\phi_j\phi_k + \text{c.c.}\right)$$
$$+ (m^2)^i{}_j\phi_i\phi_j^*. \qquad (A2)$$

The β functions for the superpotential parameters can be obtained by using superfield technique [66,67]. The obtained results are [46]

$$\beta_Y^{ijk} = Y^{p(ij}\gamma_p{}^{k)}, \qquad (A3)$$

$$\beta_\mu^{ij} = \mu^{p(i}\gamma_p{}^{j)}. \qquad (A4)$$

The exact results for the soft β functions are given by [63]

$$\beta_M = 2\mathcal{O}\left[\frac{\beta_g}{g}\right], \qquad \beta_h^{ijk} = h^{l(jk}\gamma^{i)}{}_l - 2Y^{l(jk}\gamma_1{}^{i)}{}_l,$$
$$\beta_b^{ij} = b^{l(i}\gamma^{j)}{}_l - 2\mu^{l(i}\gamma_1{}^{j)}{}_l, \qquad (A5)$$

$$(\beta_{m^2})^i{}_j = \Delta\gamma^i{}_j, \qquad (A6)$$

where γ is the matter multiplet anomalous dimension, β_g the beta function for the gauge coupling g; the $(\ldots)$ in the superscripts denote symmetrisation and

$$\mathcal{O} = Mg^2\frac{\partial}{\partial g^2} - h^{lmn}\frac{\partial}{\partial Y^{lmn}}, \qquad (A7)$$

$$(\gamma_1)^i{}_j = \mathcal{O}\gamma^i{}_j, \qquad (A8)$$

$$\Delta = 2\mathcal{O}\mathcal{O}^* + 2MM^*g^2\frac{\partial}{\partial g^2} + \left[\tilde{Y}^{lmn}\frac{\partial}{\partial Y^{lmn}} + \text{c.c.}\right] + X\frac{\partial}{\partial g}. \qquad (A9)$$

Here M is the gaugino mass and $\tilde{Y}^{ijk} = (m^2)^i{}_l Y^{jkl} + (m^2)^j{}_l Y^{ikl} + (m^2)^k{}_l Y^{ijl}$. Eqs. (A5) and (A6) hold in a class of renormalisation schemes that includes the Dimensional Reduction' (DRED')-one [68]. We take the known contributions of X from [69]:

$$X^{\text{DRED}'(1)} = -2g^3 S, \qquad (A10)$$

$$X^{\text{DRED}'(2)} = (2r)^{-1}g^3\,\text{tr}[WC(R)] - 4g^5C(G)S - 2g^5C(G)QMM^*, \qquad (A11)$$

where

$$S = r^{-1}\,\text{tr}[m^2C(R)] - MM^*C(G), \qquad (A12)$$

$$W^j{}_i = \frac{1}{2}Y_{ipq}Y^{pqn}(m^2)^j{}_n + \frac{1}{2}Y^{jpq}Y_{pqn}(m^2)^n{}_i + 2Y_{ipq}Y^{jpr}(m^2)^q{}_r + h_{ipq}h^{jpq} - 8g^2MM^*C(R)^j{}_i, \qquad (A13)$$

$C(R), C(G)$ being the quadratic Casimirs for the matter and adjoint representations, respectively, $Q = T(R) - 3C(G)$, and $rT(R) = \text{tr}[C(R)]$, r being the number of group generators.

In the following subsections, we give the anomalous dimensions and beta functions for the seesaw models of type-II and type-III so that with the help of the above equations one can calculate all RGEs at the 2-loop level.

1. The anomalous dimensions for seesaw type-II

Here and in the subsequent sections **1** denotes the 3×3 unit matrix. N_X is the number of generations of heavy field X. Furthermore, we define

$$\tilde{N}_X = N_X + N_{\bar{X}}. \qquad (A14)$$

$$\gamma_{\hat{q}}^{(1)} = -\frac{1}{30}(45g_2^2 + 80g_3^2 + g_1^2)\mathbf{1} + Y_d^\dagger Y_d + Y_u^\dagger Y_u \qquad (A15)$$

$$\gamma_{\hat{q}}^{(2)} = +\frac{4}{5}g_1^2 Y_u^\dagger Y_u - 3|\lambda_2|^2 Y_u^\dagger Y_u - 2Y_d^\dagger Y_d Y_d^\dagger Y_d - 4Y_d^\dagger Y_s Y_s^* Y_d - 2Y_d^\dagger Y_z Y_z^\dagger Y_d - 2Y_u^\dagger Y_u Y_u^\dagger Y_u + \mathbf{1}[199g_1^4 + 90g_1^2 g_2^2 + 3375g_2^4$$

$$+ 160(g_1^2 g_3^2 + 5(4g_2^2 g_3^2 - g_3^4)) + 48(125g_3^4 + g_1^4)\tilde{N}_S + (54g_1^4 + 2700g_2^4)\tilde{N}_T + (3g_1^4 + 2025g_2^4 + 2400g_3^4)\tilde{N}_Z]\frac{1}{900}$$

$$+ Y_d^\dagger Y_d\left[-3|\lambda_1|^2 - 3\text{Tr}(Y_d Y_d^\dagger) + \frac{2}{5}g_1^2 - \text{Tr}(Y_e Y_e^\dagger)\right] - 3Y_u^\dagger Y_u\text{Tr}(Y_u Y_u^\dagger) \qquad (A16)$$

$$\gamma_{\hat{l}}^{(1)} = 3(Y_z^\dagger Y_z + Y_t^* Y_t) - \frac{3}{10}(5g_2^2 + g_1^2)\mathbf{1} + Y_e^\dagger Y_e \tag{A17}$$

$$\gamma_{\hat{l}}^{(2)} = -\frac{2}{5}g_1^2 Y_z^\dagger Y_z + 16g_3^2 Y_z^\dagger Y_z + \frac{18}{5}g_1^2 Y_t^* Y_t + 12g_2^2 Y_t^* Y_t - 3|\lambda_1|^2 Y_t^* Y_t - 2Y_e^\dagger Y_e Y_e^\dagger Y_e - 6Y_z^\dagger Y_d Y_d^\dagger Y_z - 12Y_z^\dagger Y_s Y_s^* Y_z$$
$$- 6Y_z^\dagger Y_z Y_z^\dagger Y_z - 9Y_t^* Y_t Y_t^* Y_t - 3Y_t^* Y_e^T Y_e^* Y_t - 9Y_t^* Y_z^T Y_z^* Y_t + \frac{3}{100}\mathbf{1}[69g_1^4 + 30g_1^2 g_2^2 + 125g_2^4 + 16g_1^4\tilde{N}_S$$
$$+ (18g_1^4 + 100g_2^4)\tilde{N}_T + (g_1^4 + 75g_2^4)\tilde{N}_Z] + Y_e^\dagger Y_e\left[-3|\lambda_1|^2 - 3\operatorname{Tr}(Y_d Y_d^\dagger) + \frac{6}{5}g_1^2 - \operatorname{Tr}(Y_e Y_e^\dagger)\right]$$
$$- 3Y_t^* Y_t \operatorname{Tr}(Y_t Y_t^*) - 3Y_z^\dagger Y_z \operatorname{Tr}(Y_z Y_z^\dagger) \tag{A18}$$

$$\gamma_{\hat{H}_d}^{(1)} = 3|\lambda_1|^2 + 3\operatorname{Tr}(Y_d Y_d^\dagger) - \frac{3}{10}g_1^2 - \frac{3}{2}g_2^2 + \operatorname{Tr}(Y_e Y_e^\dagger) \tag{A19}$$

$$\gamma_{\hat{H}_d}^{(2)} = -12|\lambda_1^2|^4 + \frac{3}{5}|\lambda_1|^2[-15\operatorname{Tr}(Y_d Y_d^\dagger) + 20g_2^2 - 5\operatorname{Tr}(Y_e Y_e^\dagger) - 5\operatorname{Tr}(Y_t Y_t^*) + 6g_1^2] + \frac{1}{100}[207g_1^4 + 90g_1^2 g_2^2 + 375g_2^4$$
$$+ 48g_1^4\tilde{N}_S + (54g_1^4 + 300g_2^4)\tilde{N}_T + (3g_1^4 + 225g_2^4)\tilde{N}_Z - 40g_1^2\operatorname{Tr}(Y_d Y_d^\dagger)] + 16g_3^2\operatorname{Tr}(Y_d Y_d^\dagger) - 9\operatorname{Tr}(Y_d Y_d^\dagger Y_d Y_d^\dagger)$$
$$- 12\operatorname{Tr}(Y_d Y_d^\dagger Y_s Y_s^*) - 6\operatorname{Tr}(Y_d Y_d^\dagger Y_z Y_z^\dagger) - 3\operatorname{Tr}(Y_d Y_u^\dagger Y_u Y_d^\dagger) - 3\operatorname{Tr}(Y_e Y_e^\dagger Y_e Y_e^\dagger - 3\operatorname{Tr}(Y_e Y_z^\dagger Y_z Y_e^\dagger)$$
$$- 3\operatorname{Tr}(Y_e Y_t^* Y_t Y_e^\dagger) + 1.2g_1^2\operatorname{Tr}(Y_e Y_e^\dagger)) \tag{A20}$$

$$\gamma_{\hat{H}_u}^{(1)} = 3|\lambda_2|^2 - \frac{3}{10}(-10\operatorname{Tr}(Y_u Y_u^\dagger) + 5g_2^2 + g_1^2) \tag{A21}$$

$$\gamma_{\hat{H}_u}^{(2)} = \frac{1}{100}[207g_1^4 + 90g_1^2 g_2^2 + 375g_2^4 - 1200|\lambda_2|^4 + 48g_1^4\tilde{N}_S + (54g_1^4 + 300g_2^4)\tilde{N}_T + (3g_1^4 + 225g_2^4)\tilde{N}_Z$$
$$+ 60|\lambda_2|^2(-15\operatorname{Tr}(Y_u Y_u^\dagger) + 20g_2^2 + 6g_1^2) + 80g_1^2\operatorname{Tr}(Y_u Y_u^\dagger)] + 16g_3^2\operatorname{Tr}(Y_u Y_u^\dagger) - 3\operatorname{Tr}(Y_d Y_u^\dagger Y_u Y_d^\dagger)$$
$$- 9\operatorname{Tr}(Y_u Y_u^\dagger Y_u Y_u^\dagger) \tag{A22}$$

$$\gamma_{\hat{d}}^{(1)} = 2(2Y_s^* Y_s + Y_d^* Y_d^T + Y_z^* Y_z^T) - \frac{2}{15}(20g_3^2 + g_1^2)\mathbf{1} \tag{A23}$$

$$\gamma_{\hat{d}}^{(2)} = +\frac{32}{15}g_1^2 Y_s^* Y_s + \frac{80}{3}g_3^2 Y_s^* Y_s + \frac{2}{5}g_1^2 Y_z^* Y_z^T + 6g_2^2 Y_z^* Y_z^T - 2Y_d^* Y_d^T Y_d^* Y_d^T - 2Y_d^* Y_u^T Y_u^* Y_d^T - 8Y_s^* Y_d Y_d^\dagger Y_s - 16Y_s^* Y_s Y_s^* Y_s$$
$$- 8Y_s^* Y_z Y_z^\dagger Y_s - 6Y_z^* Y_t Y_t^* Y_z^T - 2Y_z^* Y_e^T Y_e^* Y_z^T - 6Y_z^* Y_z^T Y_z^* Y_z^T + \frac{1}{225}\mathbf{1}[202g_1^4 + 160g_1^2 g_3^2 - 200g_3^4$$
$$+ 12(125g_3^4 + 4g_1^4)\tilde{N}_S + 54g_1^4\tilde{N}_T + (3g_1^4 + 600g_3^4)\tilde{N}_Z] - 2Y_z^* Y_z^T\operatorname{Tr}(Y_z Y_z^\dagger) - 4Y_s^* Y_s\operatorname{Tr}(Y_s Y_s^*)$$
$$+ Y_d^* Y_d^T\left[-2\operatorname{Tr}(Y_e Y_e^\dagger) + 6g_2^2 - 6|\lambda_1|^2 - 6\operatorname{Tr}(Y_d Y_d^\dagger) + \frac{2}{5}g_1^2\right] \tag{A24}$$

$$\gamma_{\hat{u}}^{(1)} = 2Y_u^* Y_u^T - \frac{8}{15}(5g_3^2 + g_1^2)\mathbf{1} \tag{A25}$$

$$\gamma_{\hat{u}}^{(2)} = \frac{2}{225}[21\mathbf{1}(214g_1^4 + 160g_1^2 g_3^2 - 50g_3^4 + (375g_3^4 + 48g_1^4)\tilde{N}_S + 54g_1^4\tilde{N}_T + (3g_1^4 + 150g_3^4)\tilde{N}_Z)$$
$$- 45\{5(Y_u^* Y_d^T Y_d^* Y_u^T + Y_u^* Y_u^T Y_u^* Y_u^T) + Y_u^* Y_u^T(-15g_2^2 + 15|\lambda_2|^2 + 15\operatorname{Tr}(Y_u Y_u^\dagger) + g_1^2)\}] \tag{A26}$$

$$\gamma_{\hat{e}}^{(1)} = 2Y_e^* Y_e^T - \frac{6}{5}g_1^2\mathbf{1} \tag{A27}$$

$$\gamma_{\hat{e}}^{(2)} = \frac{1}{25}[3g_1^4\mathbf{1}(16\tilde{N}_S + 18\tilde{N}_T + 78 + \tilde{N}_Z)$$
$$- 10\{5(3Y_e^*Y_tY_t^*Y_e^T + 3Y_e^*Y_z^TY_z^*Y_e^T + Y_e^*Y_e^TY_e^*Y_e^T)$$
$$+ Y_e^*Y_e^T(-15g_2^2 + 15|\lambda_1|^2 + 15\,\text{Tr}(Y_dY_d^\dagger)$$
$$+ 3g_1^2 + 5\,\text{Tr}(Y_eY_e^\dagger))\}] \tag{A28}$$

$$\gamma_{\hat{T}}^{(1)} = -4g_2^2 - \frac{6}{5}g_1^2 + |\lambda_1|^2 + \text{Tr}(Y_tY_t^*) \tag{A29}$$

$$\gamma_{\hat{T}}^{(2)} = \frac{1}{25}[234g_1^4 + 240g_1^2g_2^2 + 500g_2^4 - 150|\lambda_1|^4$$
$$+ 48g_1^4\tilde{N}_S + (54g_1^4 + 200g_2^4)\tilde{N}_T + (3g_1^4 + 150g_2^4)\tilde{N}_Z$$
$$- 5|\lambda_1|^2(10\,\text{Tr}(Y_eY_e^\dagger) + 30\,\text{Tr}(Y_dY_d^\dagger) + 3g_1^2 + 5g_2^2)$$
$$- 15g_1^2\,\text{Tr}(Y_tY_t^*) - 25g_2^2\,\text{Tr}(Y_tY_t^*) - 50\,\text{Tr}(Y_eY_t^*Y_tY_e^\dagger)$$
$$- 150\,\text{Tr}(Y_tY_z^\dagger Y_zY_t^*) - 150\,\text{Tr}(Y_tY_t^*Y_tY_t^*)] \tag{A30}$$

$$\gamma_{\hat{\bar{T}}}^{(1)} = -4g_2^2 - \frac{6}{5}g_1^2 + |\lambda_2|^2 \tag{A31}$$

$$\gamma_{\hat{\bar{T}}}^{(2)} = \frac{1}{25}[234g_1^4 + 240g_1^2g_2^2 + 500g_2^4 - 150|\lambda_2|^4$$
$$+ 48g_1^4\tilde{N}_S + (54g_1^4 + 200g_2^4)\tilde{N}_T + (3g_1^4 + 150g_2^4)\tilde{N}_Z$$
$$- 5|\lambda_2|^2(30\,\text{Tr}(Y_uY_u^\dagger) + 3g_1^2 + 5g_2^2)] \tag{A32}$$

$$\gamma_{\hat{S}}^{(1)} = -\frac{4}{15}(25g_3^2 + 2g_1^2) + \text{Tr}(Y_sY_s^*) \tag{A33}$$

$$\gamma_{\hat{S}}^{(2)} = \frac{2}{225}[3(32g_1^4 + 625g_3^4)\tilde{N}_S + 2\{214g_1^4 + 400g_1^2g_3^2$$
$$+ 1375g_3^4 + 54g_1^4\tilde{N}_T + (3g_1^4 + 375g_3^4)\tilde{N}_Z$$
$$- 15g_1^2\,\text{Tr}(Y_sY_s^*) - 75g_3^2\,\text{Tr}(Y_sY_s^*)$$
$$- 225\,\text{Tr}(Y_dY_d^\dagger Y_sY_s^*) - 450\,\text{Tr}(Y_sY_s^*Y_sY_s^*)$$
$$- 225\,\text{Tr}(Y_sY_s^*Y_zY_z^\dagger)\}] \tag{A34}$$

$$\gamma_{\hat{\bar{S}}}^{(1)} = -\frac{4}{15}(25g_3^2 + 2g_1^2) \tag{A35}$$

$$\gamma_{\hat{\bar{S}}}^{(2)} = \frac{2}{225}[428g_1^4 + 800g_1^2g_3^2 + 2750g_3^4$$
$$+ 3(32g_1^4 + 625g_3^4)\tilde{N}_S + 108g_1^4\tilde{N}_T$$
$$+ (6g_1^4 + 750g_3^4)\tilde{N}_Z] \tag{A36}$$

$$\gamma_{\hat{Z}}^{(1)} = \frac{1}{30}(30\,\text{Tr}(Y_zY_z^\dagger) - 45g_2^2 - 80g_3^2 - g_1^2) \tag{A37}$$

$$\gamma_{\hat{Z}}^{(2)} = +\frac{199}{900}g_1^4 + \frac{1}{10}g_1^2g_2^2 + \frac{15}{4}g_2^4 + \frac{8}{45}g_1^2g_3^2 + 8g_2^2g_3^2$$
$$- \frac{8}{9}g_3^4 + \frac{4}{75}(125g_3^4 + g_1^4)\tilde{N}_S + \left(\frac{3}{50}g_1^4 + 3g_2^4\right)\tilde{N}_T$$
$$+ \left(\frac{1}{300}g_1^4 + \frac{9}{4}g_2^4 + \frac{8}{3}g_3^4\right)\tilde{N}_Z + \frac{2}{5}g_1^2\,\text{Tr}(Y_zY_z^\dagger)$$
$$- 2\,\text{Tr}(Y_dY_d^\dagger Y_zY_z^\dagger) - \text{Tr}(Y_eY_z^\dagger Y_zY_e^\dagger) - 4\,\text{Tr}(Y_sY_s^*Y_zY_z^\dagger)$$
$$- 3\,\text{Tr}(Y_tY_z^\dagger Y_zY_t^*) - 5\,\text{Tr}(Y_zY_z^\dagger Y_zY_z^\dagger) \tag{A38}$$

$$\gamma_{\hat{\bar{Z}}}^{(1)} = \frac{1}{30}(-45g_2^2 - 80g_3^2 - g_1^2) \tag{A39}$$

$$\gamma_{\hat{\bar{Z}}}^{(2)} = \frac{1}{900}[199g_1^4 + 90g_1^2g_2^2 + 3375g_2^4$$
$$+ 160(g_1^2g_3^2 + 20g_2^2g_3^2 - 5g_3^4)$$
$$+ 48(125g_3^4 + g_1^4)\tilde{N}_S + (54g_1^4 + 2700g_2^4)\tilde{N}_T$$
$$+ (3g_1^4 + 2025g_2^4 + 2400g_3^4)\tilde{N}_Z] \tag{A40}$$

2. Beta coefficients for the seesaw type-II at 2-loop level

$$\beta_{g_1}^{(1)} = \frac{1}{10}g_1^3(16\tilde{N}_S + 18\tilde{N}_T + 66 + \tilde{N}_Z) \tag{A41}$$

$$\beta_{g_1}^{(2)} = \frac{1}{150}g_1^3[1194g_1^2 + 810g_2^2 + 2640g_3^2$$
$$- 810(|\lambda_1|^2 + |\lambda_2|^2) + (256g_1^2 + 3200g_3^2)\tilde{N}_S$$
$$+ (648g_1^2 + 2160g_2^2)\tilde{N}_T + (g_1^2 + 45g_2^2 + 80g_3^2)\tilde{N}_Z$$
$$- 420\,\text{Tr}(Y_dY_d^\dagger) - 540\,\text{Tr}(Y_eY_e^\dagger) - 720\,\text{Tr}(Y_sY_s^*)$$
$$- 810\,\text{Tr}(Y_tY_t^*) - 780\,\text{Tr}(Y_uY_u^\dagger) - 420\,\text{Tr}(Y_zY_z^\dagger)] \tag{A42}$$

$$\beta_{g_2}^{(1)} = \frac{1}{2}g_2^3(3\tilde{N}_Z + 4\tilde{N}_T + 2) \tag{A43}$$

$$\beta_{g_2}^{(2)} = \frac{1}{10}g_2^3[18g_1^2 + 250g_2^2 + 240g_3^2 - 70|\lambda_1|^2 - 70|\lambda_2|^2$$
$$+ (48g_1^2 + 240g_2^2)\tilde{N}_T + (g_1^2 + 105g_2^2 + 80g_3^2)\tilde{N}_Z$$
$$- 60\,\text{Tr}(Y_dY_d^\dagger) - 20\,\text{Tr}(Y_eY_e^\dagger) - 70\,\text{Tr}(Y_tY_t^*)$$
$$- 60\,\text{Tr}(Y_uY_u^\dagger) - 60\,\text{Tr}(Y_zY_z^\dagger)] \tag{A44}$$

$$\beta_{g_3}^{(1)} = \frac{1}{2}g_3^3(2(-3 + \tilde{N}_Z) + 5\tilde{N}_S) \tag{A45}$$

$$\beta_{g_3}^{(2)} = \frac{1}{15}g_3^3[33g_1^2 + 135g_2^2 + 210g_3^2 + 5(145g_3^2 + 8g_1^2)\tilde{N}_S$$
$$- 135\,\text{Tr}(Y_sY_s^*) + (g_1^2 + 45g_2^2 + 170g_3^2)\tilde{N}_Z$$
$$- 60\,\text{Tr}(Y_dY_d^\dagger) - 60\,\text{Tr}(Y_uY_u^\dagger) - 60\,\text{Tr}(Y_zY_z^\dagger)] \tag{A46}$$

3. The anomalous dimensions for seesaw type-III

$$\gamma_{\hat{q}}^{(1)} = -\frac{1}{30}(45g_2^2 + 80g_3^2 + g_1^2)\mathbf{1} + Y_d^\dagger Y_d + Y_u^\dagger Y_u \tag{A47}$$

$$
\begin{aligned}
\gamma_{\hat{q}}^{(2)} = &+\frac{4}{5}g_1^2 Y_u^\dagger Y_u - 2Y_d^\dagger Y_d Y_d^\dagger Y_d - 2Y_d^\dagger Y_x^T Y_x^* Y_d - 2Y_u^\dagger Y_u Y_u^\dagger Y_u + \mathbf{1}\left[\frac{199}{900}g_1^4 + \frac{1}{10}g_1^2 g_2^2 + \frac{15}{4}g_2^4\right. \\
&+ \frac{8}{45}g_1^2 g_3^2 + 8g_2^2 g_3^2 - \frac{8}{9}g_3^4 + 8g_3^4 N_{G_M} + 3g_2^4 N_{W_M} + \left.\left(\frac{1}{12}g_1^4 + \frac{9}{4}g_2^4 + \frac{8}{3}g_3^4\right)\tilde{N}_{X_M}\right] - \frac{3}{10}Y_u^\dagger Y_u \operatorname{Tr}(Y_b Y_b^\dagger) \\
&+ Y_d^\dagger Y_d\left(-3\operatorname{Tr}(Y_d Y_d^\dagger) + \frac{2}{5}g_1^2 - \operatorname{Tr}(Y_e Y_e^\dagger)\right) - 3Y_u^\dagger Y_u \operatorname{Tr}(Y_u Y_u^\dagger) - \frac{3}{2}Y_u^\dagger Y_u \operatorname{Tr}(Y_w Y_w^\dagger) - 3Y_u^\dagger Y_u \operatorname{Tr}(Y_x Y_x^\dagger)
\end{aligned}
\tag{A48}
$$

$$\gamma_{\hat{l}}^{(1)} = \frac{1}{10}(10Y_e^\dagger Y_e + 15Y_w^\dagger Y_w - 3(5g_2^2 + g_1^2)\mathbf{1} + 3Y_b^\dagger Y_b) \tag{A49}$$

$$
\begin{aligned}
\gamma_{\hat{l}}^{(2)} = \frac{1}{200}[&240g_1^2 Y_e^\dagger Y_e + 1200g_2^2 Y_w^\dagger Y_w - 36Y_b^\dagger Y_b Y_b^\dagger Y_b - 60Y_b^\dagger Y_b Y_w^\dagger Y_w - 400Y_e^\dagger Y_e Y_e^\dagger Y_e - 45Y_w^\dagger Y_w Y_b^\dagger Y_b \\
&- 300Y_w^\dagger Y_w Y_w^\dagger Y_w + 61(100g_2^4 N_{W_M} + 125g_2^4 + 25(3g_2^4 + g_1^4)\tilde{N}_{X_M} + 30g_1^2 g_2^2 + 69g_1^4) - 18Y_b^\dagger Y_b \operatorname{Tr}(Y_b Y_b^\dagger) \\
&- 90Y_w^\dagger Y_w \operatorname{Tr}(Y_b Y_b^\dagger) - 600Y_e^\dagger Y_e \operatorname{Tr}(Y_d Y_d^\dagger) - 200Y_e^\dagger Y_e \operatorname{Tr}(Y_e Y_e^\dagger) - 180Y_b^\dagger Y_b \operatorname{Tr}(Y_u Y_u^\dagger) - 900Y_w^\dagger Y_w \operatorname{Tr}(Y_u Y_u^\dagger) \\
&- 90Y_b^\dagger Y_b \operatorname{Tr}(Y_w Y_w^\dagger) - 450Y_w^\dagger Y_w \operatorname{Tr}(Y_w Y_w^\dagger) - 180Y_b^\dagger Y_b \operatorname{Tr}(Y_x Y_x^\dagger) - 900Y_w^\dagger Y_w \operatorname{Tr}(Y_x Y_x^\dagger)]
\end{aligned}
\tag{A50}
$$

$$\gamma_{\hat{H}_d}^{(1)} = 3\operatorname{Tr}(Y_d Y_d^\dagger) - \frac{3}{10}(5g_2^2 + g_1^2) + \operatorname{Tr}(Y_e Y_e^\dagger) \tag{A51}$$

$$
\begin{aligned}
\gamma_{\hat{H}_d}^{(2)} = &+\frac{207}{100}g_1^4 + \frac{9}{10}g_1^2 g_2^2 + \frac{15}{4}g_2^4 + 3g_2^4 N_{W_M} + \frac{3}{4}(3g_2^4 + g_1^4)\tilde{N}_{X_M} - 9\operatorname{Tr}(Y_d Y_d^\dagger Y_d Y_d^\dagger) - \frac{2}{5}g_1^2 \operatorname{Tr}(Y_d Y_d^\dagger) \\
&+ 16g_3^2 \operatorname{Tr}(Y_d Y_d^\dagger) + \frac{6}{5}g_1^2 \operatorname{Tr}(Y_e Y_e^\dagger) - \frac{3}{10}\operatorname{Tr}(Y_b Y_e^\dagger Y_e Y_b^\dagger) - 6\operatorname{Tr}(Y_d Y_d^\dagger Y_x^T Y_x^*) - 3\operatorname{Tr}(Y_d Y_u^\dagger Y_u Y_d^\dagger) \\
&- 3\operatorname{Tr}(Y_e Y_e^\dagger Y_e Y_e^\dagger) - \frac{3}{2}\operatorname{Tr}(Y_e Y_w^\dagger Y_w Y_e^\dagger)
\end{aligned}
\tag{A52}
$$

$$\gamma_{\hat{H}_u}^{(1)} = -\frac{3}{10}(-10\operatorname{Tr}(Y_u Y_u^\dagger) - 10\operatorname{Tr}(Y_x Y_x^\dagger) + 5g_2^2 - 5\operatorname{Tr}(Y_w Y_w^\dagger) - \operatorname{Tr}(Y_b Y_b^\dagger) + g_1^2) \tag{A53}$$

$$
\begin{aligned}
\gamma_{\hat{H}_u}^{(2)} = &+\frac{207}{100}g_1^4 + \frac{9}{10}g_1^2 g_2^2 + \frac{15}{4}g_2^4 + 3g_2^4 N_{W_M} + \frac{3}{4}(3g_2^4 + g_1^4)\tilde{N}_{X_M} + \frac{4}{5}g_1^2 \operatorname{Tr}(Y_u Y_u^\dagger) + 16g_3^2 \operatorname{Tr}(Y_u Y_u^\dagger) + 6g_2^2 \operatorname{Tr}(Y_w Y_w^\dagger) \\
&+ 2g_1^2 \operatorname{Tr}(Y_x Y_x^\dagger) + 16g_3^2 \operatorname{Tr}(Y_x Y_x^\dagger) - \frac{3}{10}\operatorname{Tr}(Y_b Y_e^\dagger Y_e Y_b^\dagger) - \frac{57}{40}\operatorname{Tr}(Y_b Y_w^\dagger Y_w Y_b^\dagger) - 6\operatorname{Tr}(Y_d Y_d^\dagger Y_x^T Y_x^*) - 3\operatorname{Tr}(Y_d Y_u^\dagger Y_u Y_d^\dagger) \\
&- \frac{3}{2}\operatorname{Tr}(Y_e Y_w^\dagger Y_w Y_e^\dagger) - 9\operatorname{Tr}(Y_u Y_u^\dagger Y_u Y_u^\dagger) - \frac{15}{4}\operatorname{Tr}(Y_w Y_w^\dagger Y_w Y_w^\dagger) - 9\operatorname{Tr}(Y_x Y_x^\dagger Y_x Y_x^\dagger) - \frac{27}{100}\operatorname{Tr}(Y_b Y_b^\dagger Y_b Y_b^\dagger)
\end{aligned}
\tag{A54}
$$

$$\gamma_{\hat{d}}^{(1)} = 2(Y_x^\dagger Y_x + Y_d^* Y_d^T) - \frac{2}{15}(20g_3^2 + g_1^2)\mathbf{1} \tag{A55}$$

$$
\begin{aligned}
\gamma_{\hat{d}}^{(2)} = &+\frac{2}{5}g_1^2 Y_d^* Y_d^T + 6g_2^2 Y_d^* Y_d^T - 2Y_x^\dagger Y_x Y_x^\dagger Y_x - 2Y_d^* Y_d^T Y_d^* Y_d^T - 2Y_d^* Y_u^T Y_u^* Y_d^T \\
&+ \frac{1}{225}\mathbf{1}[160g_1^2 g_3^2 + 1800g_3^4 N_{G_M} - 200g_3^4 + 202g_1^4 + 75(8g_3^4 + g_1^4)\tilde{N}_{X_M}] \\
&- 6Y_d^* Y_d^T \operatorname{Tr}(Y_d Y_d^\dagger) - 2Y_d^* Y_d^T \operatorname{Tr}(Y_e Y_e^\dagger) + Y_x^\dagger Y_x(2g_1^2 - 3\operatorname{Tr}(Y_w Y_w^\dagger) \\
&+ 6g_2^2 - 6\operatorname{Tr}(Y_u Y_u^\dagger) - 6\operatorname{Tr}(Y_x Y_x^\dagger) - \frac{3}{5}\operatorname{Tr}(Y_b Y_b^\dagger))
\end{aligned}
\tag{A56}
$$

$$\gamma_{\hat{u}}^{(1)} = 2Y_u^* Y_u^T - \frac{8}{15}(5g_3^2 + g_1^2)\mathbf{1} \qquad \text{(A57)}$$

$$\gamma_{\hat{u}}^{(2)} = -2(Y_u^* Y_d^T Y_d^* Y_u^T + Y_u^* Y_u^T Y_u^* Y_u^T) + \frac{4}{225}\mathbf{1}[160g_1^2 g_3^2$$
$$+ 214g_1^4 + 450g_3^4 N_{G_M} - 50g_3^4 + 75(2g_3^2 + g_1^4)\tilde{N}_{X_M}]$$
$$- \frac{1}{5}Y_u^* Y_u^T[15\,\mathrm{Tr}(Y_w Y_w^\dagger) + 2g_1^2 - 30g_2^2$$
$$+ 30\,\mathrm{Tr}(Y_u Y_u^\dagger) + 30\,\mathrm{Tr}(Y_x Y_x^\dagger) + 3\,\mathrm{Tr}(Y_b Y_b^\dagger)]$$
$$\text{(A58)}$$

$$\gamma_{\hat{e}}^{(1)} = 2Y_e^* Y_e^T - \frac{6}{5}g_1^2 \mathbf{1} \qquad \text{(A59)}$$

$$\gamma_{\hat{e}}^{(2)} = -\frac{3}{5}Y_e^* Y_b^T Y_b^* Y_e^T - 2Y_e^* Y_e^T Y_e^* Y_e^T - 3Y_e^* Y_w^T Y_w^* Y_e^T$$
$$+ \frac{3}{25}g_1^4 \mathbf{1}(25\tilde{N}_{X_M} + 78) + Y_e^* Y_e^T\Big[-2\,\mathrm{Tr}(Y_e Y_e^\dagger)$$
$$+ 6g_2^2 - 6\,\mathrm{Tr}(Y_d Y_d^\dagger) - \frac{6}{5}g_1^2\Big] \qquad \text{(A60)}$$

$$\gamma_{\hat{W}_M}^{(1)} = -4g_2^2 \mathbf{1} + Y_w^* Y_w^T \qquad \text{(A61)}$$

$$\gamma_{\hat{W}_M}^{(2)} = +2g_2^4 \mathbf{1}(3\tilde{N}_{X_M} + 4N_{W_M} + 10) + \frac{1}{10}[-3Y_w^* Y_b^T Y_b^* Y_w^T$$
$$- 10Y_w^* Y_e^T Y_e^* Y_w^T - 15Y_w^* Y_w^T Y_w^* Y_w^T + Y_w^* Y_w^T\{-10g_2^2$$
$$- 15\,\mathrm{Tr}(Y_w Y_w^\dagger) - 30\,\mathrm{Tr}(Y_u Y_u^\dagger) - 30\,\mathrm{Tr}(Y_x Y_x^\dagger)$$
$$- 3\,\mathrm{Tr}(Y_b Y_b^\dagger) + 6g_1^2\}] \qquad \text{(A62)}$$

$$\gamma_{\hat{G}_M}^{(1)} = -6g_3^2 \mathbf{1} \qquad \text{(A63)}$$

$$\gamma_{\hat{G}_M}^{(2)} = 6g_3^4 \mathbf{1}(3N_{G_M} + 3 + \tilde{N}_{X_M}) \qquad \text{(A64)}$$

$$\gamma_{\hat{B}_M}^{(1)} = \frac{3}{5}Y_b^* Y_b^T \qquad \text{(A65)}$$

$$\gamma_{\hat{B}_M}^{(2)} = \frac{3}{50}[-3Y_b^* Y_b^T Y_b^* Y_b^T - 5(2Y_b^* Y_e^T Y_e^* Y_b^T$$
$$+ 3Y_b^* Y_w^T Y_w^* Y_b^T) + 3Y_b^* Y_b^T\{10g_2^2 - 10\,\mathrm{Tr}(Y_u Y_u^\dagger)$$
$$- 10\,\mathrm{Tr}(Y_x Y_x^\dagger) + 2g_1^2 - 5\,\mathrm{Tr}(Y_w Y_w^\dagger) - \mathrm{Tr}(Y_b Y_b^\dagger)\}]$$
$$\text{(A66)}$$

$$\gamma_{\hat{X}_M}^{(1)} = -\frac{1}{6}(16g_3^2 + 5g_1^2 + 9g_2^2)\mathbf{1} \qquad \text{(A67)}$$

$$\gamma_{\hat{X}_M}^{(2)} = \frac{1}{36}\mathbf{1}[223g_1^4 + 90g_1^2 g_2^2 + 135g_2^4 + 160g_1^2 g_3^2$$
$$+ 288(g_2^2 g_3^2 + g_3^4 N_{G_M}) - 32g_3^4 + 108g_2^4 N_{W_M}$$
$$+ (75g_1^4 + 81g_2^4 + 96g_3^4)\tilde{N}_{X_M}] \qquad \text{(A68)}$$

$$\gamma_{\hat{\bar{X}}_M}^{(1)} = \frac{1}{6}(-(16g_3^2 + 5g_1^2 + 9g_2^2)\mathbf{1} + 6Y_x^* Y_x^T) \qquad \text{(A69)}$$

$$\gamma_{\hat{\bar{X}}_M}^{(2)} = +\frac{1}{36}\mathbf{1}[223g_1^4 + 90g_1^2 g_2^2 + 135g_2^4 + 160g_1^2 g_3^2$$
$$+ 288(g_2^2 g_3^2 + g_3^4 N_{G_M}) - 32g_3^4 + 108g_2^4 N_{W_M}$$
$$+ (75g_1^4 + 81g_2^4 + 96g_3^4)\tilde{N}_{X_M}]$$
$$+ \frac{1}{10}[-20(Y_x^* Y_d Y_d^\dagger Y_x^T + Y_x^* Y_x^T Y_x^* Y_x^T)$$
$$- Y_x^* Y_x^T\{15\,\mathrm{Tr}(Y_w Y_w^\dagger) + 30\,\mathrm{Tr}(Y_u Y_u^\dagger)$$
$$+ 30\,\mathrm{Tr}(Y_x Y_x^\dagger) + 3\,\mathrm{Tr}(Y_b Y_b^\dagger) + 4g_1^2\}] \qquad \text{(A70)}$$

4. Beta coefficients for the seesaw type-III at 2-loop level

$$\beta_{g_1}^{(1)} = \frac{1}{10}g_1^3(25\tilde{N}_{X_M} + 66) \qquad \text{(A71)}$$

$$\beta_{g_1}^{(2)} = \frac{1}{150}g_1^3[125(16g_3^2 + 5g_1^2 + 9g_2^2)\tilde{N}_{X_M} + 6\{199g_1^2$$
$$+ 135g_2^2 + 440g_3^2 - 9\,\mathrm{Tr}(Y_b Y_b^\dagger) - 70\,\mathrm{Tr}(Y_d Y_d^\dagger)$$
$$- 90\,\mathrm{Tr}(Y_e Y_e^\dagger) - 130\,\mathrm{Tr}(Y_u Y_u^\dagger) - 60\,\mathrm{Tr}(Y_w Y_w^\dagger)$$
$$- 190\,\mathrm{Tr}(Y_x Y_x^\dagger)\}] \qquad \text{(A72)}$$

$$\beta_{g_2}^{(1)} = \frac{1}{2}g_2^3(3\tilde{N}_{X_M} + 4N_{W_M} + 2) \qquad \text{(A73)}$$

$$\beta_{g_2}^{(2)} = \frac{1}{30}g_2^3[54g_1^2 + 750g_2^2 + 720(g_3^2 + g_2^2 N_{W_M})$$
$$+ 15(16g_3^2 + 21g_2^2 + 5g_1^2)\tilde{N}_{X_M} - 18\,\mathrm{Tr}(Y_b Y_b^\dagger)$$
$$- 280\,\mathrm{Tr}(Y_w Y_w^\dagger) - 60\,\mathrm{Tr}(Y_e Y_e^\dagger) - 180(\mathrm{Tr}(Y_d Y_d^\dagger)$$
$$+ \mathrm{Tr}(Y_u Y_u^\dagger) + \mathrm{Tr}(Y_x Y_x^\dagger))] \qquad \text{(A74)}$$

$$\beta_{g_3}^{(1)} = g_3^3(3N_{G_M} - 3 + \tilde{N}_{X_M}) \qquad \text{(A75)}$$

$$\beta_{g_3}^{(2)} = \frac{1}{15}g_3^3[33g_1^2 + 135g_2^2 + 210g_3^2 + 810g_3^2 N_{G_M}$$
$$+ 5(34g_3^2 + 5g_1^2 + 9g_2^2)\tilde{N}_{X_M} + 170g_3^2 N_{\bar{X}_M}$$
$$- 60\,\mathrm{Tr}(Y_d Y_d^\dagger) - 60\,\mathrm{Tr}(Y_u Y_u^\dagger) - 60\,\mathrm{Tr}(Y_x Y_x^\dagger)] \qquad \text{(A76)}$$

[1] Y. Fukuda *et al.* (Super-Kamiokande Collaboration), Phys. Rev. Lett. **81**, 1562 (1998).

[2] Q. R. Ahmad *et al.* (SNO), Phys. Rev. Lett. **89**, 011301 (2002).

[3] K. Eguchi *et al.* (KamLAND), Phys. Rev. Lett. **90**, 021802 (2003).

[4] KamLAND Collaboration, Phys. Rev. Lett. **100**, 221803 (2008).

[5] T. Schwetz, M. A. Tortola, and J. W. F. Valle, New J. Phys. **10**, 113011 (2008). Version 3 on the arXive is updated with data until Feb 2010

[6] S. Weinberg, Phys. Rev. Lett. **43**, 1566 (1979); Phys. Rev. D **22**, 1694 (1980).

[7] E. Ma, Phys. Rev. Lett. **81**, 1171 (1998).

[8] P. Minkowski, Phys. Lett. B **67**, 421 (1977).

[9] T. Yanagida, in *KEK Lectures*, edited by O. Sawada and A. Sugamoto (KEK, Tsukuba, Japan, 1979); M. Gell-Mann, P. Ramond, and R. Slansky, in *Supergravity*, edited by P. van Niewenhuizen and D. Freedman (North Holland, Amsterdam, 1979).

[10] R. N. Mohapatra and G. Senjanovic, Phys. Rev. Lett. **44**, 912 (1980).

[11] J. Schechter and J. W. F. Valle, Phys. Rev. D **22**, 2227 (1980).

[12] T. P. Cheng and L. F. Li, Phys. Rev. D **22**, 2860 (1980).

[13] R. Foot, H. Lew, X. G. He, and G. C. Joshi, Z. Phys. C **44**, 441 (1989).

[14] A. Rossi, Phys. Rev. D **66**, 075003 (2002).

[15] M. R. Buckley and H. Murayama, Phys. Rev. Lett. **97**, 231801 (2006).

[16] J. Hisano, T. Moroi, K. Tobe, and M. Yamaguchi, Phys. Rev. D **53**, 2442 (1996).

[17] J. R. Ellis, J. Hisano, M. Raidal, and Y. Shimizu, Phys. Rev. D **66**, 115013 (2002).

[18] F. Deppisch, H. Paes, A. Redelbach, R. Rückl, and Y. Shimizu, Eur. Phys. J. C **28**, 365 (2003).

[19] S. T. Petcov, S. Profumo, Y. Takanishi, and C. E. Yaguna, Nucl. Phys. **B676**, 453 (2004).

[20] E. Arganda and M. J. Herrero, Phys. Rev. D **73**, 055003 (2006).

[21] S. T. Petcov, T. Shindou, and Y. Takanishi, Nucl. Phys. **B738**, 219 (2006).

[22] S. Antusch, E. Arganda, M. J. Herrero, and A. M. Teixeira, J. High Energy Phys. 11 (2006) 090.

[23] F. Deppisch and J. W. F. Valle, Phys. Rev. D **72**, 036001 (2005).

[24] J. Hisano, T. Moroi, K. Tobe, M. Yamaguchi, and T. Yanagida, Phys. Lett. B **357**, 579 (1995).

[25] M. Hirsch, J. W. F. Valle, W. Porod, J. C. Romao, and A. Villanova del Moral, Phys. Rev. D **78**, 013006 (2008).

[26] E. Arganda, M. J. Herrero, and A. M. Teixeira, J. High Energy Phys. 10 (2007) 104.

[27] F. Deppisch, T. S. Kosmas, and J. W. F. Valle, Nucl. Phys. **B752**, 80 (2006).

[28] M. Hirsch, S. Kaneko, and W. Porod, Phys. Rev. D **78**, 093004 (2008).

[29] C. Biggio and L. Calibbi, J. High Energy Phys. 10 (2010) 037.

[30] J. Hisano, M. M. Nojiri, Y. Shimizu, and M. Tanaka, Phys. Rev. D **60**, 055008 (1999).

[31] J. N. Esteves, J. C. Romao, A. Villanova del Moral, M. Hirsch, J. W. F. Valle, and W. Porod, J. High Energy Phys. 05 (2009) 003.

[32] G. A. Blair, W. Porod, and P. M. Zerwas, Eur. Phys. J. C **27**, 263 (2003).

[33] A. Freitas, W. Porod, and P. M. Zerwas, Phys. Rev. D **72**, 115002 (2005).

[34] F. Deppisch, A. Freitas, W. Porod, and P. M. Zerwas, Phys. Rev. D **77**, 075009 (2008).

[35] B. C. Allanach, J. P. Conlon, and C. G. Lester, Phys. Rev. D **77**, 076006 (2008).

[36] A. Abada, A. J. R. Figueiredo, J. C. Romao, and A. M. Teixeira, J. High Energy Phys. 10 (2010) 104.

[37] E. Komatsu *et al.*, arXiv:1001.4538.

[38] K. Griest and D. Seckel, Phys. Rev. D **43**, 3191 (1991).

[39] H. Baer, C. Balazs, and A. Belyaev, J. High Energy Phys. 03 (2002) 042.

[40] J. L. Feng, K. T. Matchev, and T. Moroi, Phys. Rev. D **61**, 075005 (2000).

[41] M. Drees and M. M. Nojiri, Phys. Rev. D **47**, 376 (1993).

[42] J. N. Esteves, S. Kaneko, J. C. Romao, M. Hirsch, and W. Porod, Phys. Rev. D **80**, 095003 (2009).

[43] F. Staub, arXiv:0806.0538.

[44] F. Staub, Comput. Phys. Commun. **181**, 1077 (2010).

[45] F. Staub, arXiv:1002.0840.

[46] S. P. Martin and M. T. Vaughn, Phys. Rev. D **50**, 2282 (1994); **78**, 039903(E) (2008).

[47] F. Borzumati and T. Yamashita, Prog. Theor. Phys. **124**, 761 (2010).

[48] S. K. Kang, T. Morozumi, and N. Yokozaki, J. High Energy Phys. 11 (2010) 061.

[49] J. A. Casas and A. Ibarra, Nucl. Phys. **B618**, 171 (2001).

[50] L. Calibbi, M. Frigerio, S. Lavignac, and A. Romanino, J. High Energy Phys. 12 (2009) 057.

[51] L. Calibbi, Y. Mambrini, and S. K. Vempati, J. High Energy Phys. 09 (2007) 081.

[52] B. C. Allanach *et al.*, Eur. Phys. J. C **25**, 113 (2002).

[53] W. Martens, L. Mihaila, J. Salomon, and M. Steinhauser, Phys. Rev. D **82**. 095013 (2010).

[54] W. Porod, Comput. Phys. Commun. **153**, 275 (2003).

[55] For the latetst version of SPheno, see the web page http://www.physik.uni-wuerzburg.de/~porod/SPheno.html .

[56] S. Antusch and M. Ratz, J. High Energy Phys. 07 (2002) 059.

[57] P. F. Harrison, D. H. Perkins, and W. G. Scott, Phys. Lett. B **530**, 167 (2002).

[58] C. Amsler *et al.* (Particle Data Group), Phys. Lett. B **667**, 1 (2008).

[59] G. Belanger, F. Boudjema, A. Pukhov, and A. Semenov, Comput. Phys. Commun. **176**, 367 (2007).

[60] B. C. Allanach, A. Djouadi, J. L. Kneur, W. Porod, and P. Slavich, J. High Energy Phys. 09 (2004) 044.

[61] S. Heinemeyer, W. Hollik, H. Rzehak, and G. Weiglein, Eur. Phys. J. C **39**, 465 (2005).

[62] LEPSUSYWG, ALEPH, DELPHI, L3, and OPAL experiments, note LEPSUSYWG/01-03.1, http://lepsusy.web.cern.ch/lepsusy/Welcome.html.

[63] I. Jack, D. R. T. Jones, and A. Pickering, Phys. Lett. B **426**, 73 (1998).

[64] Y. Yamada, Phys. Rev. D **50**, 3537 (1994).

[65] http://theorie.physik.uni-wuerzburg.de/~fnstaub/ supplementary.html.

[66] P. C. West, Phys. Lett. B **137**, 371 (1984).

[67] D. R. T. Jones and L. Mezincescu, Phys. Lett. B **138**, 293 (1984).

[68] I. Jack, D. R. T. Jones, S. P. Martin, M. T. Vaughn, and Y. Yamada, Phys. Rev. D **50**, R5481 (1994).

[69] I. Jack, D. R. T. Jones, and A. Pickering, Phys. Lett. B **432**, 114 (1998).